

Spatio-temporal variability of Arctic summer temperatures over the past two millennia

Johannes P. Werner¹, Dmitry V. Divine^{2,3}, Fredrik Charpentier Ljungqvist^{4,5}, Tine Nilsen³, and Pierre Francus^{6,7}

¹Bjerknes Centre for Climate Research and Department for Earth Science, University of Bergen, PO Box 7803, N-5020 Bergen, Norway

²Norwegian Polar Institute, FRAM Centre, N-9296 Tromsø, Norway.

³Department of Mathematics and Statistics, University of Tromsø – The Arctic University of Norway, N-9037, Norway

⁴Department of History, Stockholm University, SE-106 91 Stockholm, Sweden

⁵Bolin Centre for Climate Research, Stockholm University, SE-106 91 Stockholm, Sweden

⁶Centre - Eau Terre Environnement, Institut National de la Recherche Scientifique, 490 rue de la couronne, Québec, QC G1K 9A9, Canada

⁷GEOTOP Research Center, Montréal, H3C 3P8, Canada

Correspondence to: J.P. Werner (johannes.werner@geo.uib.no)

Abstract.

In this article, the first spatially resolved and millennium-length summer (June–August) temperature reconstruction over the Arctic and Subarctic domain (north of 60° N) is presented. It is based on a set of 44 annually dated temperature sensitive proxy archives of various types, mainly from the updated and revised PAGES2k database supplemented with 6 new recently updated proxy records. As a major advance, an extension of the Bayesian BARCAST climate field (CF) reconstruction technique provides a means to treat climate archives with dating uncertainties. In total over 600 independent realisations of the temperature CF were generated, enabling further analyses to be carried out in a probabilistic framework. The new seasonal CF reconstruction for the Arctic region can be shown to be skilful for the majority of the terrestrial nodes. The decrease in the proxy data density back in time however limits the analyses in the spatial domain to the period after 750 CE, while the spatially averaged reconstruction covers the entire time interval of 1–2002 CE. The analysis of basic features of the reconstructed seasonal CF focuses on the regional expression of past major climate anomalies in order to uncover the potential of the new product for studying Common Era temperature variability in the region.

The long-term, centennial to millennial, evolution of the reconstructed temperature is in good agreement with a general pattern that was inferred in recent studies for the Arctic and its sub-regions. The reconstruction shows a pronounced Medieval Climate Anomaly (MCA, here, ca. 920–1060 CE), which was characterised by a sequence of extremely warm decades over the whole domain. The medieval warming was followed by a gradual cooling into the Little Ice Age (LIA), with 1766–1865 CE as the longest centennial-scale cold period, culminating around 1811–1820 CE for most of the target region.

While our analysis shows that the peak MCA summer temperatures were as high as in the late 20th and early 21st century, the spatial coherence of extreme years over the last decades of the reconstruction (1980s onwards) seems unprecedented at least back until 750 CE. However, statistical testing could not provide conclusive support of the contemporary warming to exceed

the peak of the MCA in terms of the pan-Arctic mean summer temperatures: neither can the reconstruction be extended reliably past 2002 CE due to lack of proxy data and thus the most recent warming is not captured, nor is it (from a statistical viewpoint) advisable to directly compare the reconstruction and instrumental data.

1 Introduction

25 During the past decades, the Arctic has experienced a more rapid and pronounced temperature increase than most other parts
of the world. The dramatically shrinking extent of Arctic sea-ice in recent years – with a decline in both minimum extent in
summer and maximum area in winter – accompanied by a transition to a younger and thinner sea ice cover, is often interpreted
as the clearest and most unambiguous evidence of anthropogenic global warming (Comiso et al., 2008; Perovich et al., 2008;
Serreze et al., 2007; Maslanik et al., 2011; Meier et al., 2014). Additionally, the Arctic region is of utmost importance in the
30 context of global climate and global climate change. Reduction in perennial sea ice cover leads to increased heat transport
northward (Müller et al., 2012; Smedsrud et al., 2008), as well as changes the Arctic energy balance due to positive albedo
feedbacks (Curry et al., 1995; Miller et al., 2010; Perovich et al., 2002, 2011). Melting of permafrost can release methane
(CH₄), a more efficient greenhouse gas than carbon dioxide (CO₂), and likewise gives a positive feedback that may further
amplify the temperature increase (O’Connor et al., 2010; Shakhova et al., 2010). Even partial melting of the Greenland inland
35 ice cap and/or the numerous smaller high-latitude glaciers would significantly raise the global sea level and threaten to flood
low-laying coastal regions around the world (Grinsted et al., 2010; Vermeer and Rahmstorf, 2009).

The instrumental temperature record is too short and spatially sparse to assess whether this recent warming and the accom-
panying sea-ice reduction experienced in the Arctic region so far, fall outside the range of natural variability on centennial
to millennial time-scales. Moreover, general circulation models have limited capabilities in reliably simulating Arctic climate
40 change on centennial time-scale and beyond (IPCC, 2013). The simplified parametrisations of dynamic and thermodynamic
sea-ice processes, and the limited skills in describing ocean–sea-ice–atmosphere energy exchange, in particular in modelling
polar clouds and oceanic heat flux, is especially evident from the lack of skill in reproducing the present-day rapid loss of
Arctic sea-ice (e.g. Hunke et al., 2010). Hence both the possible unprecedented nature of the on-going Arctic warming during
the Common Era (CE, the last 2000 years) and the relative role of anthropogenic and natural forcings driving the process
45 are difficult to fully assess without a longer perspective from palaeoclimate proxy-based temperature reconstructions. Thus
palaeoclimate data that can be used for understanding the range of natural climate variability in the Arctic region over long
time-scales are needed, together with methods that integrate different types of information from a variety of palaeoclimate
archives.

Since the 1990s, several multi-proxy reconstructions of Arctic and Subarctic (usually 90–60° N) temperatures have been
50 published. The first one of those was the multi-proxy reconstruction by Overpeck et al. (1997), who compiled 29 proxy records
from lake sediment, tree-ring, glacier, and marine sediment records to present a decadal resolved uncalibrated index of tem-
perature variability since 1600 CE. They found that the highest temperatures in the Arctic region since 1600 CE occurred after
1920 CE. Kaufman et al. (2009) published the first quantitative multi-proxy reconstruction of summer temperature variability
in the Arctic (90–60° N) during the past 2,000-year at decadal resolution using the composite-plus-scaling method. This study
55 concluded that the 20th century warming reverses a long-term orbitally driven summer cooling and that the mid- and late 20th
century temperatures were the highest in the past two millennia.

Shi et al. (2012) published the first annually resolved multi-proxy summer (June–August) temperature reconstruction for the Arctic region, extending back to 600 CE, based on a set of 22 proxy records with annual resolution. They utilised a novel ensemble reconstruction method that combined the traditional composite-plus-scale method – known to underestimate low-frequency variability (e.g. von Storch et al., 2004) – and the LOC (local regression) method of Christiansen (2011) that exaggerates the high-frequency variability (c.f. e.g. Christiansen and Ljungqvist, 2017). The reconstructed amplitude of the centennial-scale summer temperature variability was rather dampened and found to be less than 0.5° C but with large year-to-year and decadal-to-decadal variability. Shi et al. (2012) found a clear cold anomaly 630 to 770 CE, a peak warming ca. 950 to 1050 CE, and overall relatively cold conditions ca. 1200–1900 CE. However, three distinctly warmer periods during the Little Ice Age were reconstructed ca. 1470–1510, 1550–1570, and 1750–1770 CE. Contrary to Kaufman et al. (2009), Shi et al. (2012) found peak medieval Arctic summer temperatures in the 10th century to be approximately equal to recent Arctic summer temperatures.

Tingley and Huybers (2013) used BARCAST (Bayesian Algorithm for Reconstructing Climate Anomalies in Space and Time Tingley and Huybers, 2010a), a method based on Bayesian inference of hierarchical models (see also sec. 3), to reconstruct surface-air temperatures of the last 600 years over land north of 60° N. Their reconstruction is mostly based on the proxy dataset collected by the PAGES 2k Consortium (2013). They found that while the recent decades were the warmest over the last 600 years, the actual inter-annual variability has remained effectively constant. Much of the data (most of the ice core and lake sediment records) used therein are common with the work presented here, with a few updated records (see section 2.2, and PAGES 2k Consortium, 2017) and a few additional proxies (such as the tree ring width series).

Hanhijärvi et al. (2013) presented a 2000-year long annual mean temperature reconstruction for the North Atlantic sector of the Arctic (north of 60° N and between 50° W and 30° E) using 27 proxy records of various types, resolution and length employing the novel Pairwise Comparison (PaiCo) method. Their reconstruction reveals centennial-scale temperature variations of an amplitude of over 1°C, with a distinct Roman Warm Period, warm Medieval Climate Anomaly and 20th century warming. A somewhat indistinct Dark Age Cold Period is found in the middle of the first millennium CE, whereas a very clear and persistently cold Little Ice Age extends from the mid-13th century until the turn of the 20th century, with the lowest temperatures in the 19th century. Peak temperatures during the Roman Warm Period and the Medieval Climate Anomaly were found to equal recent temperatures in the the North Atlantic sector of the Arctic. The PAGES 2k Consortium (2013) extended the PaiCo reconstruction to cover the whole Arctic (60–90° N), using 67 proxy records of various types, resolution and length to reconstruct annual mean temperature variations over the past two millennia. They reconstructed a generally relatively warm first millennium CE, followed by a relatively indistinct Medieval Climate Anomaly, and a relatively cold Little Ice Age from ca. 1250 CE to 1900 CE. The amplitude of the reconstructed low-frequency temperature variability in the whole Arctic by the PAGES 2k Consortium (2013) is smaller than that reconstructed for only the North Atlantic sector of the Arctic by Hanhijärvi et al. (2013). A revised Arctic2k reconstruction was subsequently published by McKay and Kaufman (2014), using an updated and corrected proxy database containing 59 records, showing a larger long-term cooling trend and is on average ca. 0.5°C warmer prior to ca. 1250 CE than reported by PAGES 2k Consortium (2013). Peak temperatures during the Roman Warm Period and the Medieval Climate Anomaly thus approximately equal recent temperatures in McKay and Kaufman (2014) as in

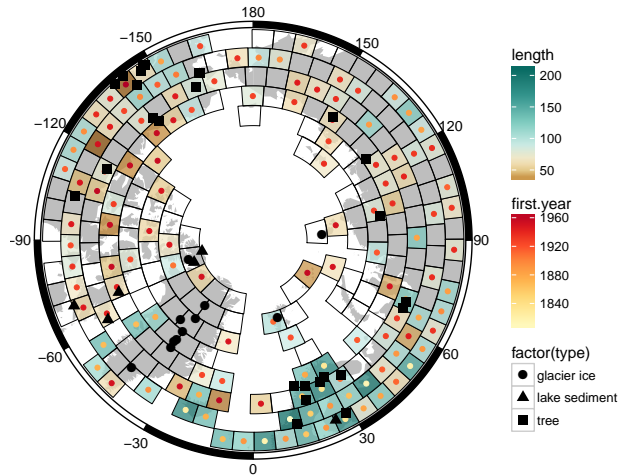


Figure 1. Distribution of input data. Length (fill of quadrilaterals) and first year (coloured circles) of the regridded instrumental data. Symbols show the locations and type of used proxy data (PAGES 2k Consortium, 2017). The reconstruction target area are all grid cells marked with wire frames.

Shi et al. (2012) and Hanhijärvi et al. (2013), instead of being much lower as in the Arctic2k reconstruction by the PAGES 2k Consortium (2013).

This study is mostly comparable with that of Tingley and Huybers (2013): our method is an update of theirs (Tingley and Huybers, 2010a; Werner and Tingley, 2015), and the proxy network is an update of the PAGES2k database (PAGES 2k Consortium, 2017). There are, however, a few notable differences: i) the CF reconstruction is performed on an equal area grid (land only), which should be more suitable for a spatially homogeneous process – especially at high latitudes. ii) This target gridded instrumental dataset is directly derived from meteorological observation data without any interpolation over grid cell boundaries. iii) The gridded reconstruction goes back into the first millennium CE. iiiii) The proxy dataset is larger and more extensively screened, and v) the age uncertainties of the proxies used are respected. Thus, the propagation of uncertainties from proxy data to the final reconstruction product is more complete. vi) Additionally, while Tingley and Huybers (2013) use a single set of parameters for all proxies of one type, these are estimated here for each individual record. This potentially removes spurious precision at proxy sites responding less strong to the seasonal temperature anomalies, and should increase the precision at locations with stronger climate response.

The following section provides a short overview of the used instrumental and palaeoclimate proxy data. The quality of the input data and their distribution in space and time play a strong role in the reconstruction process and for the reconstruction reliability (see e.g. Wang et al., 2015).

2.1 Instrumental data

110 Several different gridded data sets for Earth surface air temperatures (SAT) are available from different research groups, derived from different subsets of instrumental data and presented on different types of grids. Most datasets, like e.g. CRUTEM4 (Jones et al., 2012) or CRU TS3 (Harris et al., 2014) are presented on a regular equilateral grid, such as a $5^\circ \times 5^\circ$ grid. Such a regular grid exhibits severe shortcomings when analysing data close to the poles, as the grid cells become very narrow in meridional direction and almost triangular shaped. One data set, the Berkeley Earth Surface Temperature (BEST) (Rohde et al., 2013),
115 is offered on a $1^\circ \times 1^\circ$ grid as well as an equal area grid. While the latter would be a good fit for the process level model of BARCAST (c.f. sec. 3), an analysis revealed that this version of the dataset shows long distance correlations over our region of interest that might be deemed unphysical: the correlation length is in the order of the region size and the cross correlation between grid cells contains oscillatory parts with respect to the distance between the cells. The latter, especially, might be artefacts of the regridding and interpolation process.

120 Thus a new gridded instrumental data set is generated for this study. The instrumental data for the CRU TS3.24 (Harris et al., 2014) dataset were downloaded from the CRU website http://browse.ceda.ac.uk/browse/badc/cru/data/cru_ts/cru_ts_3.24.01. First, the data were converted into anomalies for the period 1801–2016 CE, using the method of Tingley (2012). The equal area target grid is taken from Leopardi (2006). To construct the gridded data, the instrumental data within each grid cell were averaged, using the variance adjustment scheme described by Frank et al. (2006). We aimed at retaining the variability that a
125 single instrumental record in the grid cell would exhibit. This is a compromise between an actual grid-cell wide average and the limited spatio-temporal availability of instrumental data in high latitudes. In contrast to other regridding methods, no data was shared across grid cells by a prescribed spatial covariance structure or spatial interpolation algorithm. While some proxies (e.g. the tree-ring maximum latewood density record from Northern Scandinavia by Esper et al., 2012) represent larger, grid-cell sized regions rather than point estimates (see the discussion in Luterbacher et al., 2016), none are large-scale regional averages
130 (such as the Central European documentary reconstruction of Dobrovolný et al., 2010, used by Luterbacher et al. 2016). In contrast to (Tingley and Huybers, 2010a, b; Werner et al., 2013) the data was not normalised to have unit standard deviation prior to running the BARCAST sampler.

As can be seen in Figure 1, the resulting instrumental dataset is very sparse in space and time. While ordinary reconstruction methods would indeed struggle with such input data, the advantage of the BARCAST method and the extension used here is
135 that presence and absence of observations are explicitly modelled. The reconstruction target region are land mass (continent and islands) containing grid cells only (wire frames in Fig. 1). This is necessary due to the constraints of the chosen reconstruction

method (Tingley and Huybers, 2010a; Werner and Tingley, 2015), more specifically due the homogeneous process level model, which describes the temperature evolution on the grid cell level.

2.2 Proxy data

140 The proxy records (black symbols in Fig. 1) mostly come from the current version (2.0.0) of the PAGES 2k Consortium (2017) temperature data base, with 6 recently updated ice core records from Greenland with revised and synchronised chronologies. The data set contains several types of natural archives (tree-rings, ice-cores and marine or terrestrial sediments) and proxy measurements (such as ring width and stable isotopes). Thus the data is sensitive to different seasons, and on different time-scales – partly due to different resolutions and the evaluation procedures, but also owed to the processes generating the archives.

145 All data north of 60° N contained in the database were selected, with an a priori aim of including all annually resolved records.

As the PAGES 2k Consortium (2017) set out to generate a very inclusive data set, the need arose to again scrutinise the data. A few records were excluded (c.f. table A1), as they did not meet the required response characteristics on actual annual time-scales. Additionally, data was divided into two classes: absolutely and precisely dated tree ring chronologies, and layer-counted proxies with age uncertainties. The latter comprises varved lacustrine sediments and ice core data. In contrast to the procedure

150 outlined by Luterbacher et al. (2016) tree-ring width measurements are not treated differently from maximum latewood density data, although the spectral properties should in principle warrant this separation (Zhang et al., 2015; Esper et al., 2015; Büntgen et al., 2015).

All of the proxy records used in this study are derived from annually banded archives. While tree-ring records are compiled by cross-referencing a number of cores for each period, there is usually very limited replication of ice-cores or varved lake sediments. Thus, these archives can (and usually do) contain age uncertainties (c.f. Sigl et al., 2015) which need to be taken into account. Fortunately, the chosen method (Werner and Tingley, 2015) is able to deal with this issue, provided an ensemble of age models is given for each proxy. Appendix D1 details how these age models are generated. As the majority of the proxy data is more sensitive to summer or growing season temperatures, the target season for the reconstruction is the climatological summer season (the months from June to August, JJA) rather than the annual mean temperature.

160 3 Reconstruction method: BARCAST+AMS

Werner and Tingley (2015) published an extension to the BARCAST method. It extends the work of Tingley and Huybers (2010a), providing a means to treat climate archives with dating uncertainties. The original method has been used in a collection of pseudo-proxy experiments (Tingley and Huybers, 2010b; Werner et al., 2013; Gómez-Navarro et al., 2015), as well as climate field reconstructions over the Arctic (Tingley and Huybers, 2013), Europe (Luterbacher et al., 2016) and Asia (Zhang et al.).

165 The method uses a hierarchy of stochastic models to describe the spatio-temporal evolution of the target climate field (here: temperatures) $C_t \in \mathbb{R}^N$ at N different locations throughout time t , and the dependence of the observations $O_t \in \mathbb{R}^N$ (proxy

data as well as instrumental data) on it:

$$\begin{aligned}
C_{t+1} - \mu &= \alpha (C_t - \mu) + \epsilon_t \\
\epsilon_t &\sim \mathcal{N}(\mathbf{0}, \Sigma) \quad (\text{independent}) \\
\Sigma_{i,j} &= \sigma^2 \exp(-\phi|x_i - x_j|),
\end{aligned}
\tag{1a}$$

170 The process level is thus AR(1) (1st order auto-regressive) in time, with an overall mean μ and the coefficient α modelling the temporal persistence. The year-to-year (or rather summer-to-summer) innovations have an exponentially (with distance between locations x_i and x_j) decreasing spatial persistence that is homogeneous in space. The spatial e-folding distance is $1/\phi$. The climate is thus persistent in space and time, and information is shared across these dimensions. This is critical in constraining age models (see discussion in Werner and Tingley, 2015). The climate process C is never directly observed without error (latent process). The observations are modelled as a noisy linear response function:

$$\begin{aligned}
175 \quad O_t &= \beta_0 + \beta_1 \cdot \mathbf{H}_t \cdot C_t + e_t \\
\epsilon_t &\sim \mathcal{N}(\mathbf{0}, \tau^2 \cdot \mathbf{I}) \quad (\text{independent}).
\end{aligned}
\tag{1b}$$

The parameters $(\beta_0, \beta_1, \tau^2, \mathbf{H}_t)$ are assumed to be different for each location with observations, while in the past one set of parameters was assigned to each proxy type (e. g., tree ring widths, ice layer thickness or isotopic values) (Tingley and Huybers, 2013). The instrumental observations are assumed to be unbiased and on the correct scale, so that, for this type of observation $\beta_0 = 0$ and $\beta_1 = 1$. The selection matrix \mathbf{H}_t is composed of zeros and ones, and selects out at time step t the locations for which 180 there are proxy observations of a given type. That is, each proxy observation is assumed to be linear in the corresponding local, in time and space, value of the climate. While interannual temperatures roughly follow a normal distribution in our target region (Tingley and Huybers, 2013), a variable like varve thickness is positive only. These variables are transformed using inverse quantile transformation (e.g. Emile-Geay and Tingley, 2016) to include them easily into the reconstruction.

This data-level model is then refined to include dating uncertainties. To this end, Werner and Tingley (2015) consider the 185 dependence of the local observations O_s on the local climate:

$$\begin{aligned}
O_s | \mathcal{T}, C_s &= \beta_0 + \beta_1 \cdot \Lambda_s^T \cdot C_s + e_s \\
e_s &\sim \mathcal{N}(\mathbf{0}, \tau^2 \cdot \mathbf{I}) \quad (\text{independent}).
\end{aligned}
\tag{1c}$$

The vector e_s is a time series of independent normal errors at location s (c.f. e_t from Eq. (1b)). In analogy to \mathbf{H}_t in Eq. (1b), Λ_s^T is a selection matrix of zeros and ones that picks out the elements of the vector C_s corresponding to elements of O_s , and is dependent on the age depth model (ADM) \mathcal{T} .

190 From these model equations, conditional posteriors for the climate field and all of the parameters (climate field and instrumental / proxy observations) are calculated. Then, a Metropolis-Coupled Markov-chain Monte Carlo (MC)³ sampler (Altekar et al., 2004; Earl and Deem, 2005; Li et al., 2009) is used to iteratively draw solutions from these posteriors, see (Tingley and Huybers, 2010a; Werner and Tingley, 2015) for details and implementations. In the version implemented here, BARCAST is slightly modified. While Tingley and Huybers (2013) used a single set of response parameters $(\beta_0, \beta_1, \tau^2)$ for all data of one

195 type, while Luterbacher et al. (2016) actually set up a separate observation matrix with a set of parameters for each single proxy, the code is updated for this study. The response parameters are now vectors. While this slows down the computations and also the convergence there is no good reason to assume that all proxies of one type respond in the same way across the whole domain and with known differences in proxy quality. This has been discussed already by Luterbacher et al. (2016), where two proxies that were initially in the PAGES2k database (PAGES 2k Consortium, 2013) proved to contain no clear temperature
200 signal (see also changes in the updated database PAGES 2k Consortium, 2017) and were thus removed.

The reconstruction code is run in 4 chains for 8000 iterations without the age model selection code enabled. By then, the chains have clearly settled to a stable state, and the potential scale reduction factor (Gelman's \hat{R}) indicates convergence of the parameters ($|\hat{R} - 1| < 0.1$). Then, the (MC)³ code of Werner and Tingley (2015) is enabled, and the age models are varied. While this was not necessary in the work of Werner and Tingley (2015), the real world data is much sparser, noisier and does
205 not follow the exact prescribed stochastic model (1a–1c). While this additional step helps speed up convergence it can cause the algorithm to strongly favour one set of age models. This can be checked by analysing the mixing properties over the age models in the heated chains (see discussion in Werner and Tingley, 2015). As noted therein, there is a tradeoff between the switching efficiency and the number of chains. With the used infrastructure, 4 chains using 2 cores each (for parallel linear algebra using the OpenBLAS library <http://www.openblas.net>) were deemed a reasonable compromise.

210 3.1 Reconstruction Quality

The reconstruction calibration and validation statistics are shown in appendix A. It has been shown that some of the commonly used measures, like the Coefficient of Efficiency and the Reduction of Error (Cook et al., 1994) are not proper scoring rules and should be avoided in such an ensemble based probabilistic framework (Gneiting and Raftery, 2007). Thus, reconstruction skill is assessed using the $\overline{\text{CRPS}}_{\text{pot}}$ (potential average Continuous Ranked Probability Score, which is akin to the Mean Absolute
215 Error of a deterministic forecast, see Gneiting and Raftery (2007)) as well as the Reliability score (the validity of the uncertainty bands, Hersbach, 2000). Additionally, a probabilistic ensemble based version of the Coefficient of Efficiency and the Reduction of Error are constructed from these (see appendix A).

Both the $\overline{\text{CRPS}}_{\text{pot}}$ as well as the Reliability score show a decent reconstruction quality (Figure A1 top row). The $\overline{\text{CRPS}}_{\text{pot}}$ on average shows a mismatch of 0.2°C (0.4°C) in the calibration (validation) interval and the Reliability is mostly better
220 than 0.2°C . This is in the order of the noise strength that the reconstruction code attributed to the instrumental observations. Additionally, the probabilistic ensemble based version of the coefficient of efficiency and the reduction of error show a skillful reconstruction in most grid cells containing instrumental temperature data – at least in regions where proxy and instrumental data are present over most of the validation period. Note that the quality of the instrumental data, or rather the representativeness of (often) a single meteorological station record can be debated. In fact, in contrast to other BARCAST based reconstructions
225 the one presented here shows a substantial ($\tau_I^2 \approx 0.25^\circ\text{C}^2$) noise level for the instrumental data. As other gridded instrumental datasets employ spatial interpolation processes these are generally smoother in space than the gridded instrumental dataset generated for this study. Thus these gridded products are by design closer to the spatial characteristics of the process model in Eq. (1a).

Another means of assessing the reconstruction quality is to check the variability or spread of the different ensemble members
230 in space and time (see appendix B). The effect of the spatially and temporally sparse data can easily be seen in Figures A2 and
A3, clearly indicating the increased uncertainties back in time and in space in the absence of proxy data. This analysis hints that
while there could still be skill left in the mean Arctic summer temperature reconstruction in the first centuries CE, the precision
of the spatial reconstruction rapidly decreases in areas that become more data sparse. While the reconstruction over the regions
with local proxy data present – such as Fennoscandia – remains reliable, a time-varying reconstruction domain (or rather,
235 domain over which the reconstruction is analysed) would be beyond the scope of this paper. Thus the gridded reconstruction
is only shown back to 750 CE. However, for single analyses over data rich regions the full reconstruction period (1–2002 CE)
can in principle be used.

Additionally, the spectral properties of both the reconstruction and the proxy input data are analysed (c.f. appendix C). Not
all proxies contain signal on centennial or longer time scales, and the reconstruction method explicitly describes year-to-year
240 summer temperatures as an AR(1) process. Thus, the reconstruction shows properties of an AR(1) process over most of the
reconstruction domain (cf. also Nilsen et al.). However, when comparing the area averaged temperature reconstructions against
other multiproxy reconstruction data one can still see similar variability on centennial and longer time-scales (see Figure 3).

4 Results

In the following sections the resulting reconstruction is presented. First, the Arctic average is analysed and compared against
245 other studies from the same region. Two periods of interest are identified in the reconstruction before the instrumental period:
the warm MCA around 920–1060 CE and the following LIA which in this reconstruction culminated in the the early 19th
century. These then provide a context for the current warming of the Arctic. A detailed analysis of an earlier extended warm
period that can be associated with the Roman Warm Period (RWP) is omitted due to a higher uncertainty of the derived
reconstruction prior to 750 CE. Yet it is acknowledged that the scales of the detected warming could be comparable to the
250 following episodes that occurred later during the MCA. Finally, the spatial variability of the reconstructed temperature field is
explored, with a focus on the most extreme periods.

4.1 Mean Arctic Results

The ensemble mean of the area averaged summer temperature reconstruction is shown in the bottom half of Figure 2 as the
pointwise (year-to-year summers) ensemble mean (heavy blue line). The first millennium CE shows a mean reconstruction
255 that exhibits an apparent change in variability. This is caused by the increased variability between the different ensemble
members and thus by the reduction in proxy data coverage back in time. The effect of the spatial proxy data coverage on the
reconstruction intra-ensemble variance is further discussed in Appendix B.

The new spatially averaged SAT reconstruction shows a pronounced variability on a broad range of time-scales. The longer-
term, centennial to millennial, evolution of the reconstructed SAT demonstrates a reasonably good agreement with a general

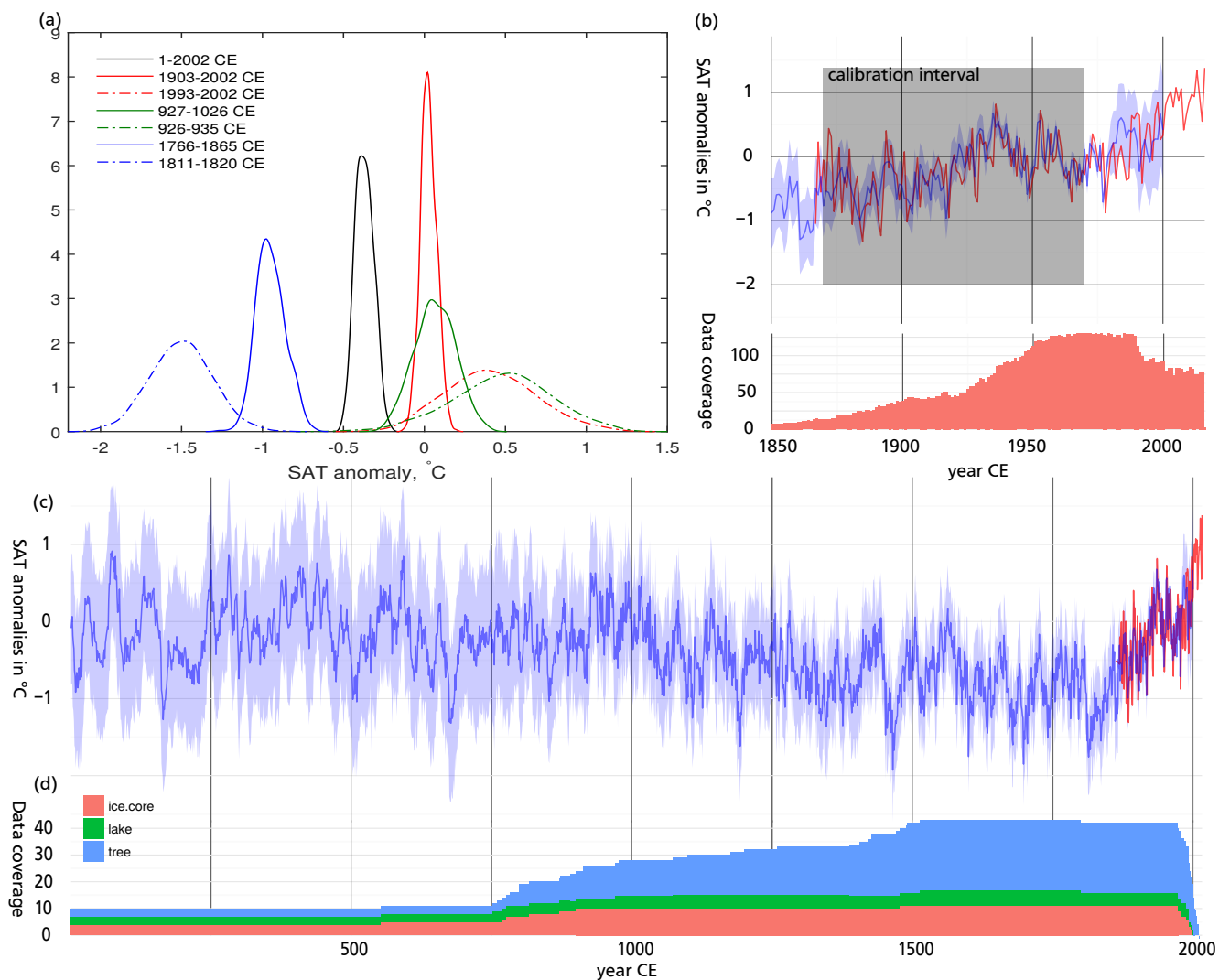


Figure 2. a) Ensemble-based mean Arctic summer (June–August) SAT (land only) anomaly probability density for the three selected centennial-scale and three decadal-scale time periods. The periods presented correspond to the coldest and warmest century- and decade-long periods of the LIA and MCA together with CWP. The actual probability densities are estimated using the Gaussian kernel density function. b) Arctic (land only) average summer temperature anomalies over the instrumental period and number of instrumental observations available. Grey box denotes the calibration interval. c) Ensemble-based spatially averaged time variability of the seasonal SAT probability distribution over the reconstruction period. Blue line: ensemble mean, shading: (pointwise) 95% posterior, red line: instrumental data. Note that before 1870 CE the number of instrumental observations rapidly decreases. d) Number of proxies by archive type over time.

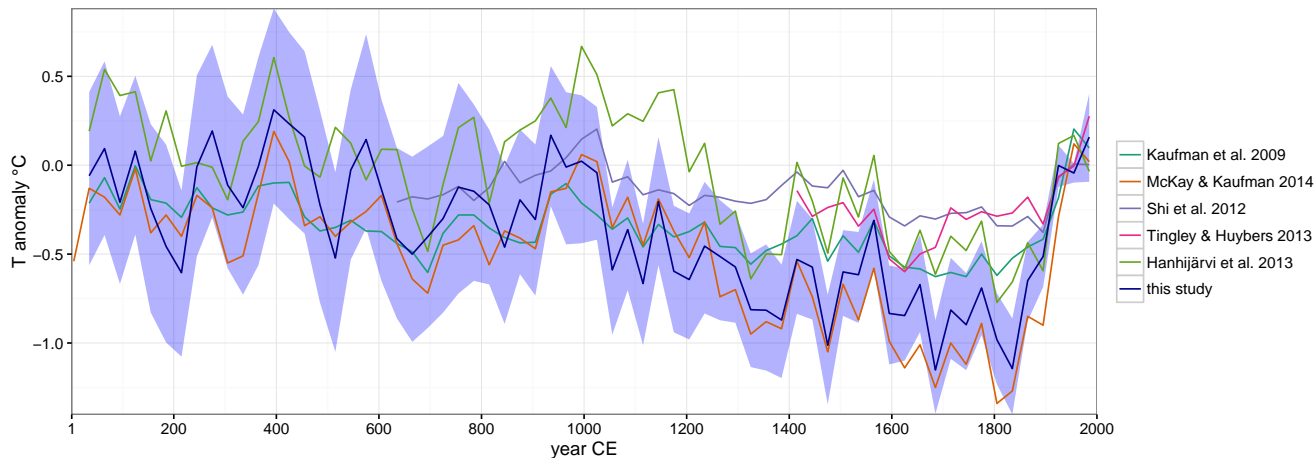


Figure 3. Comparison of this reconstruction (with 95% confidence band) with other reconstructions. 30 year averages. Note that McKay and Kaufman (2014) target annual temperatures and Hanhijärvi et al. (2013) reconstruct the North Atlantic sector of the Arctic (50° W–30° E).

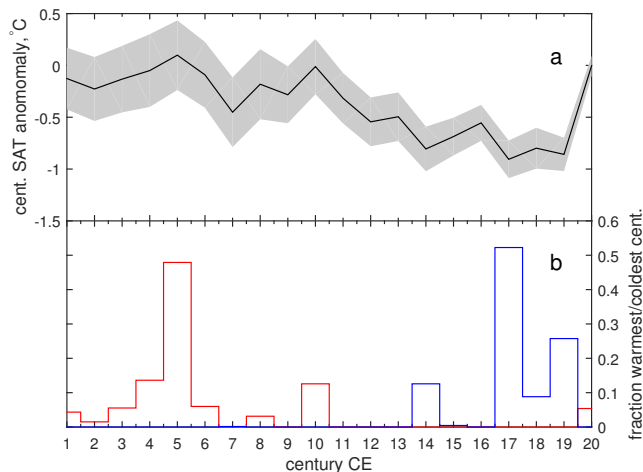


Figure 4. (a) Ensemble-averaged century and spatial mean Arctic SAT (solid black) with the respective ± 2 standard deviations highlighted gray; (b) Mean Arctic SAT ensemble-based fraction warmest (red) and coldest (blue) centuries.

260 pattern that was inferred in previous temperature reconstructions for the Arctic and its sub-regions (Figure 3). Throughout most
of the reconstruction period, the Arctic SAT anomaly shows an overall orbital forcing-driven cooling trend.

Superimposed on the trend are three major centennial to multi-centennial scale anomalies: a warm period in the 4th and 5th
centuries CE broadly associated with a relatively late phase of the Roman Warm Period (RWP), the Medieval Climate Anomaly
– a warm period during the 10th and 11th centuries CE, and the two phases of the cold Little Ice Age between ca. 1100–1450 CE
265 and 1600–1900 CE. Figure 4 further demonstrates that the three aforementioned major climate anomalies together with the most

recent period are associated with the likely warmest and coldest centuries in the Arctic over the last 2000 years. In particular, the 17th and 19th centuries CE with (within the uncertainty) similar ranged mean SAT anomalies of $-0.9 \pm 0.1^\circ\text{C}$ appear coldest in the ensemble average (Fig. 4a) and are also ranked coldest in 52% and 25% of the ensemble members, respectively. While the 5th century with a SAT anomaly of $0.1 \pm 0.2^\circ\text{C}$ appears warmest in 48% reconstruction members over the 2000 years, this
270 inference should be considered with caution due to a higher reconstruction uncertainty for this data sparse pre-750 CE period. For the later period with better proxy coverage, the 10th century CE, accommodating the MCA with the ensemble average mean SAT anomaly of $0.0 \pm 0.1^\circ\text{C}$, along with the 20th century (SAT anomaly of $0.0 \pm 0.05^\circ\text{C}$) share the rank of the two warmest centuries over the last 1200 years in the Arctic, which is in line with other studies (e.g. Ljungqvist et al., 2012, 2016).

The slow millennial-scale cooling is finally terminated by the contemporary warming which is clearly identifiable since the
275 middle of the 19th century. Figure 3 suggests that the LIA cooling is less pronounced in the new reconstruction compared with the same period reconstructed by McKay and Kaufman (2014), though the uncertainty intervals mostly overlap with their mean results. A likely explanation of this difference is the effect of targeting the summer season (as in our study) compared to annual mean in the reconstruction of McKay and Kaufman (2014). Throughout the LIA sea-ice cover has most likely experienced a pan-Arctic expansion as evidenced by proxy studies (e.g. Belt et al., 2010; Kinnard et al., 2011; Berben et al.,
280 2014; Miettinen et al., 2015) and also supported by documentary evidence for the last phase of the LIA (Divine and Dick, 2006; Walsh et al., 2017). Such sea ice expansion would lead to an increased continentality of the climate in most of the study domain, implying larger summer to winter SAT contrasts (see e.g. Grinsted et al., 2006, for Svalbard). This has potential effects on differently targeted reconstructions and the inferred magnitude of LIA cooling. The new reconstruction, however, shows larger low-frequency temperature variability than those reconstructed by Shi et al. (2012) or Tingley and Huybers (2013).

We further explore the transient features in the spatial mean reconstruction ensemble using the modified scale space method
285 SiZer (Significance of Zero Crossings of the Derivative) (Chaudhuri and Marron, 1997). The original technique uses a local linear regression kernel-based estimator to produce a family of non-parametric smooth curves for the target data series for a range of kernel bandwidths (h). Assessment of the statistical significance of the scale-dependent features in the observed data, such as the local linear trend estimate, is then provided based on the inferred variability in the data and the quantile specified.

The original SiZer summarizes the data analysis results in a map which highlights the locations in “scale” (*here*: the variability time scale) and “space” (*here*: the point in time) where the slope of a smoothed version of the unknown true underlying
290 curve is significantly positive or negative. The modification of SiZer used in this paper utilises the additional amount of information that is available via the ensemble of reconstructions. As the analysis is repeated for all individual members of the reconstruction ensemble, both the variability of the estimated slope of the smoothed curve and the spread in slope significance
295 for a certain scale and point in time can be tested. This approach therefore enables the assessment of the robustness of features detected as significant to be made across the entire range of independent and equally likely reconstructions.

Figure 5a presents results of the analysis highlighting the time scales and periods where at least 90% of the ensemble members exhibit statistically significant changes. Results suggest that given the proxy network configuration and BARCAST settings used, the overall millennial scale cooling trend as well as the MCA, LIA and CWP, appear as statistically significant
300 features in the majority of the ensemble members. The MCA to LIA transition together with the onset of the CWP are the

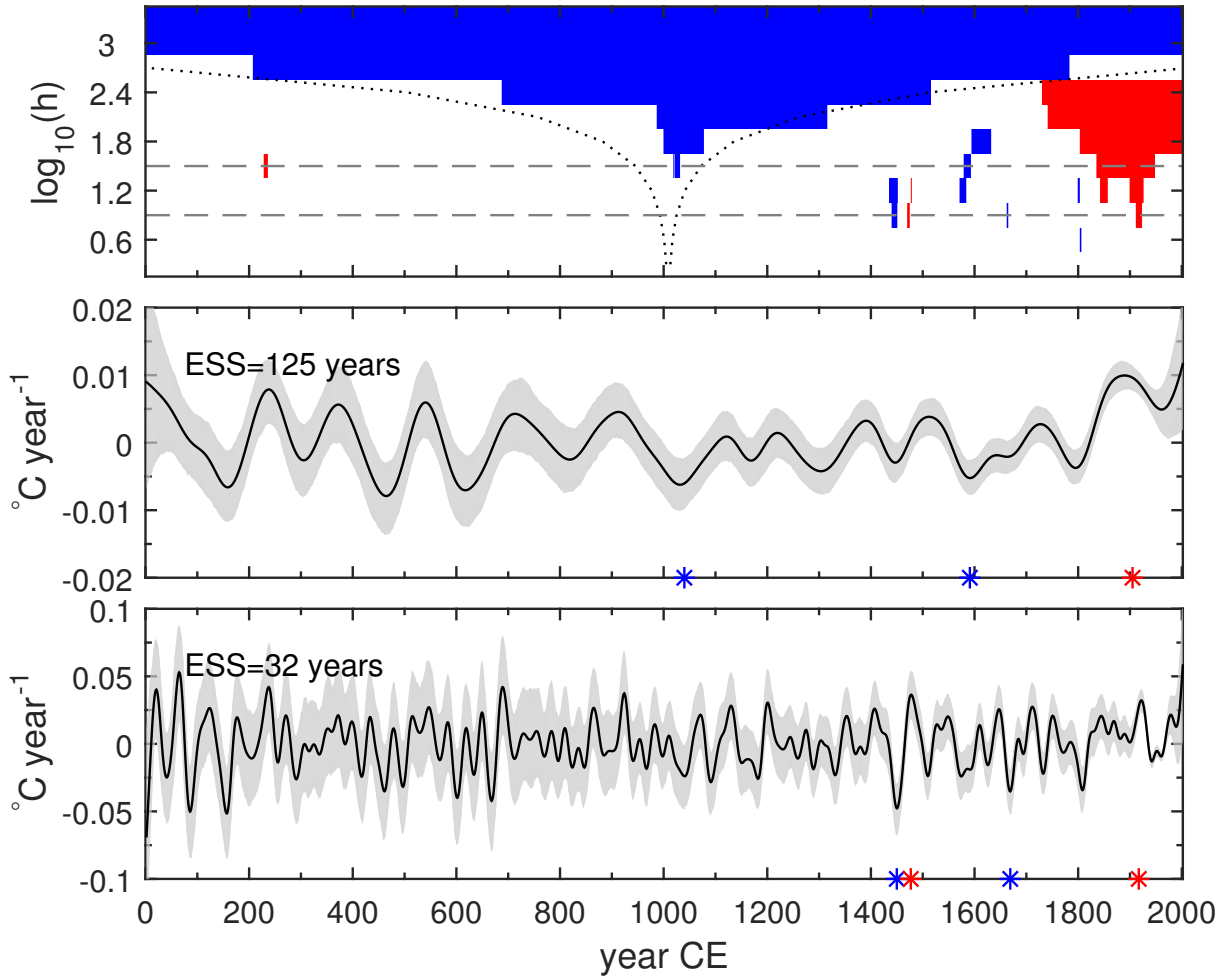


Figure 5. (a) Modified SiZer map of the spatial mean reconstructed SAT with colors red/blue marking the locations in scale (variability time scale) and space (time in this particular case) where the fraction of ensemble members exhibiting statistically significant warming/cooling exceeds 90%; the parallel distance between the dotted lines indicate the effective size of the smoothing kernel used for a particular scale and hence gives an idea of the corresponding time scale involved at that level of smoothing; Solid lines in (b) and (c) show derivatives of local linear smooth lines together with the respective double standard deviation ranges (highlighted gray) for the two selected kernel bandwidths $\log_{10}(h) = \{0.9, 1.5\}$ with effective sample sizes of about 125 and 32 years, also marked as dashes in panel (a). Blue/red asterisks in (b,c) mark the timings of the maxima in the rates of cooling/warming discussed in the text.

two coherent changes apparent on the broad range of timescales considered, down to a multidecadal scale. In particular, the initial phase of the LIA-related cooling is centered already at ca. 1030 CE and flagged significant at a range of timescales from centennial to nearly millennial. We note also that for the centennial timescale, Figure 5a points to the onset of a statistically significant warming during the 1840s CE. This would justify using 1850 CE as the cutoff year for inferring the longer term tendencies in the reconstruction prior to the CWP. Later, the period of 1917-1928 CE marks an ensemble-coherent warming trend in the terrestrial Arctic on the scale of about 30 years, which clearly links it to the early 20th century warming.

The statistically significant changes that are coherent across the reconstruction ensemble are four cooling and one warming episodes revealed at the timescales of 30-100 years and centered at 1450 CE, 1591 CE, 1669 CE, 1810 CE (cooling) and 1477 CE (warming). In order to assess the magnitude and timings of the most rapid changes for the two selected kernel bandwidths of $\log_{10}(h) = \{0.9, 1.5\}$, the derivatives of the respective kernel smooths for each ensemble member are calculated. The bandwidths selected correspond to the effective samples sizes of about 30 and 120 years and are hence representative of the three-decadal and centennial scale variations. Figure 5b,c shows the associated rates of changes as the ensemble mean together with the respective 95% CI.

The two largest statistically significant cooling rates in the entire ensemble with average temperature changes of $-1.5 \pm 0.4^{\circ}\text{C}$ and $-1.1 \pm 0.4^{\circ}\text{C}$ over three decades are registered at 1450 CE and 1669 CE, respectively, while a recovery after the first cooling centered at 1477 CE featured a warming of $1.2 \pm 0.4^{\circ}\text{C}$ over a similar 30 year time period. In terms of the rate of changes attained, the first cooling/warming episode appears unique over the 2000-year-long reconstruction, including one of the coldest decades in the reconstruction ensemble. At the highlighted centennial timescale, the most rapid changes are the MCA to LIA transition with a cooling of $-0.8 \pm 0.3^{\circ}\text{C}$ centered at 1040 CE, the cooling towards one of the LIA SAT minima at 1577 CE with $-0.7 \pm 0.2^{\circ}\text{C}$, followed by the transition to the CWP centered at 1905 CE with an average warming of $1.2 \pm 0.2^{\circ}\text{C}$ over ca. 120 years, which is also the largest centennial scale warming rate detected in the entire ensemble. Note that the intra-ensemble variations hinder a robust detection of statistically significant changes common for the majority of the spatial mean reconstruction ensemble members at the timescales shorter than three decades, with the cooling towards the absolute decadal minimum of the record at 1811-1820 CE being the only remarkable exception. The same applies to the pre-750 CE period that appears highly variable on a range of scales when the reconstructions are considered individually, but show no single episode that is localised in time across all ensemble members. The latter is related to a much reduced density of the multiproxy network for the considered period (see discussion in Werner et al., 2013), and due to the age model selection code, which would delocalise events in time (see Werner and Tingley, 2015, for details). Given the sparse proxy network before 750 CE, and a correlation length in the order of 1500 km, this clearly highlights the need for proxy data to be extended back in time.

The spatial pattern of millennial scale trends in the reconstructed Arctic SAT is further explored in Figure 6. The period of 1-1850 CE is considered as a reference period to enable comparison with the earlier studies. The results for the magnitude of the millennial scale cooling in the spatial mean reconstruction are in line with the previous studies, although the new reconstruction tends to agree best with McKay and Kaufman (2014) (see Figure 6b). While for the ensemble- and the reconstruction domain average the rate of cooling attains $-0.05 \pm 0.01^{\circ}\text{C}/\text{century}$, which results in an overall temperature decrease of about -0.9°C

during 1–1850 CE, the analysis reveals that this long term cooling trend seems spatially inhomogeneous. In particular, the largest magnitude of the millennial-scale cooling of up to $-0.13 \pm 0.02^\circ\text{C}/\text{century}$ yielding an up to a -2.4°C temperature decrease over the period of 1-1850 CE is registered in the region between $0-30^\circ\text{E}$ and $10-170^\circ\text{W}$, and only this domain actually contains proxies covering the full Common Era. Averaging over the longitudes similarly suggests that the largest cooling over the period preceding the contemporary warming has likely occurred in the region encompassing Greenland and the Canadian Arctic between $30-120^\circ\text{W}$. At the same time, much less pronounced negative trends with an overall cooling of less than -0.4°C over 1–1850 CE are detected in most of the Eurasian region within $30-180^\circ\text{E}$. This is statistically significant only in a few locations. The results outside the proxy-data rich regions are mostly reflective of the overall mean cooling trend of the remaining proxies; any in depth analysis needs (by design of the reconstruction method) to be limited to locations closer than about one or at most two e-folding lengths (ca. 1500 km) to the proxy data.

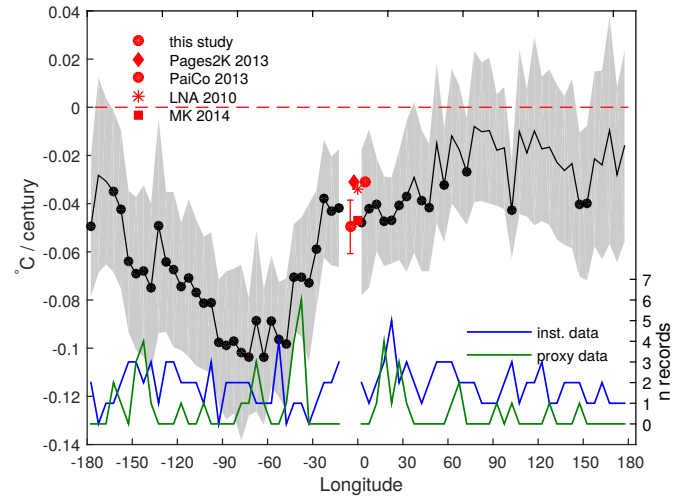
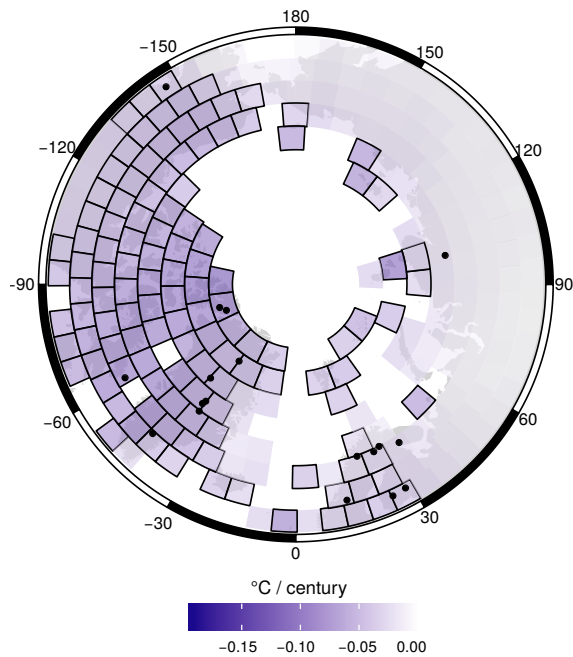
Since the gridded reconstruction is limited to the time after 750 CE, the results above need to be interpreted carefully, especially more than about 1500 km away from any proxy data. Thus, the bottom half of Fig. 6 presents a similar analysis for the time span of 750–1850 CE. The revealed pattern suggests a more even cooling throughout the reconstruction domain with circum-Arctic trend magnitudes similar within the uncertainty estimate.

4.2 Contemporary Arctic warming in the context of MCA and LIA climate anomalies

Comparing the magnitude and spatial extent of past warm periods featuring similar settings in external forcing with the present-day warming is of major importance, since it provides possible limits for the scales of naturally forced climate fluctuations. Figures 2 and 3 suggest that in the new reconstruction the period of 900-1050 CE, typically associated with the peak of the MCA, shows up at least similarly warm as the reconstruction for the late 20th and early 21st century, although the instrumental data suggest much warmer temperatures in the last decade (2006–2015 CE). This is in accordance with the conclusions reached previously in Shi et al. (2012), Hanhijärvi et al. (2013), and McKay and Kaufman (2014). The Arctic mean SAT reconstruction before about 750 CE has much higher uncertainties, and robustly identifying warm periods becomes more difficult. Especially in contrast to the reconstruction by Hanhijärvi et al. (2013) the Roman times around the first and second century CE do not show up as particularly warm in the circum-Arctic mean, which is also reflected in the analyses presented in the previous section. Note that their reconstruction was limited to the North Atlantic sector of the Arctic, and thus a direct comparison is difficult. Additionally the spatial skill of the reconstruction decreases back in time as the proxy data becomes sparser (see appendix B), and spatial averages thus result in higher uncertainties and the ensemble average will be closer to the overall mean. Taking these uncertainties into consideration, the focus will thus be on comparing the more tightly constrained MCA and LIA anomalies with the contemporary warm period.

The warmest century-long period of the mean SAT reconstruction after 750 CE associated with the MCA occupies most of the 10th century CE (927–1026 CE). The peak decade-long warmth of the MCA occurred during 926-935 CE, when the reconstructed spatial mean SAT anomaly attains $0.48 \pm 0.31^\circ\text{C}$. The timing of the coldest centennial-scale period of the LIA, specifically the 1766–1865 CE, broadly associates it with a Dalton grand solar minimum. This period also contains the coldest decadal-long event in the reconstruction detected during 1811–1820 CE with the mean Arctic ensemble based temperature

1-1850 CE



750-1850 CE

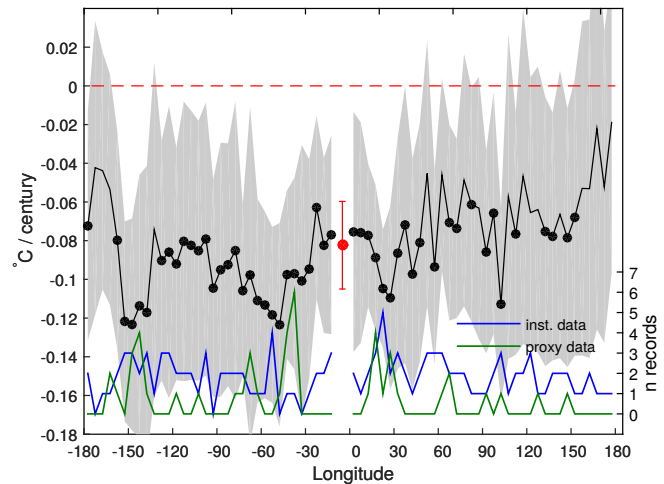
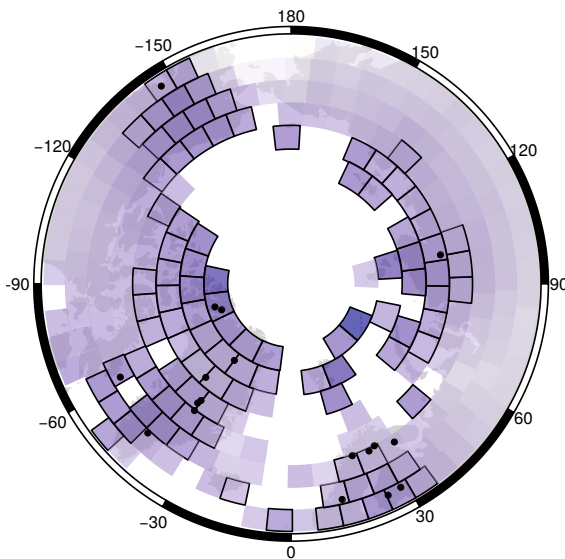


Figure 6. (a) Ensemble-averaged spatial linear trends over the period 1–1850 CE in $^{\circ}\text{C}/\text{century}$; black dots mark proxy locations, quadrilaterals mark locations where the trend is statistically significant for more than 95% ensemble members. (b) Ensemble-averaged meridional trends in the latitude-averaged reconstruction over the period 1–1850 CE (solid black line); meridional averaging over the 5° segments and zonal over the terrestrial nodes is applied to each reconstruction ensemble member. Grey shading highlights the $\pm 2 \times \text{std}$ interval on the estimated trend magnitude derived from the ensemble of spatially averaged reconstructions. Black circles indicate the meridional sectors where the trend is statistically significant. Solid green and blue lines show the number of proxy and instrumental records in each 5° longitudinal sector. For comparison, the pan-Arctic trend estimates for the same period are shown red: PAGES 2k Consortium (2013), PaiCo 2013 and LNA 2010 (both: Hanhijärvi et al., 2013), MK 2014 (McKay and Kaufman, 2014) and for this study. Panels (c), and (d) show the analysis repeated for the period 750–1850 CE.

370 anomaly of $-1.5 \pm 0.2^\circ\text{C}$. This cold decade also coincides with the period of increased volcanic activity, with two major tropical eruptions of 1808/1809 CE and Tambora 1815 CE. The second coldest decade of the LIA with the SAT anomaly of $-1.4 \pm 0.2^\circ\text{C}$ has likely occurred during 1463–1472 CE, also following strong volcanic forcing.

Figure 2a presents the ensemble-based probability densities (pdf) of the spatially averaged across the reconstruction domain mean SAT anomalies for the six selected reconstruction sub-periods. These are the three selected century-long periods of 927–1026 CE, 1766–1865 CE and 1903–2002 CE, representing both the aforementioned warmest and the coldest century-long 375 periods of the record after 750 CE as well as the last century-long period, the second warmest of the reconstruction, which includes the Contemporary Warm Period (CWP, in this study since 1978 CE onwards). For comparison, the same pdf for the entire reconstruction period is also presented. To further highlight the contrasts between the mean and extreme climate states, pdfs for the three shorter decadal-scale intervals corresponding to the anomalously warm and cold periods of 926-935 CE, 380 1811–1820 CE and 1993–2002 CE (see also Subsection 4.3 for details) are displayed. The chosen decade of the CWP is the second warmest on average in the record after the MCA in the considered reconstruction period with a SAT anomaly of $0.41 \pm 0.28^\circ\text{C}$, followed in rank by a warm decade of the early 20th century warming 1930–1939 CE, not shown here). The maps of spatial mean SAT anomalies for these periods follow in Figure 7.

Comparing the coldest phase of the LIA with a mean centennial-scale SAT anomaly of $-0.94 \pm 0.09^\circ\text{C}$ vs. the MCA 385 $0.07 \pm 0.13^\circ\text{C}$ and the last century of the reconstruction (SAT anomaly: $0.01 \pm 0.05^\circ\text{C}$) emphasises the difference between the extreme warm and cold century-long periods in terms of the pan-Arctic summer temperature probability density. Figure 2a suggests that the centennial-scale maximum of the MCA could be at least as warm as the period 1903–2002 CE, although a reduction of proxy data after the 1990s likely introduces a cold bias when estimating present-day warming in the reconstruction.

In order to quantitatively test the significance of the observed reconstructed differences in SAT anomalies between the 390 selected periods, the two-sample *t*-test is used on the samples of the derived distributions. During the testing procedure the realisations from different ensemble members of the Arctic SAT annual means are not pooled. Rather, the respective pdfs for the selected periods are derived for every individual ensemble member of the reconstructed SAT. The procedure uses bootstrap estimates of the pdf for the period (MCA and CWP) averages derived from 100 independent draws. The two-sample *t*-test with separate variances is applied to test the null-hypothesis of the two samples associated with the two different warm periods 395 to originate from two normal distributions with equal means and unknown and non-equal variances. Using a one-tailed *t*-test should then provide information on whether the MCA was on average warmer or colder than the last 100 years. The test statistics for each ensemble member is then collected and analysed.

The testing results for a two-tailed test with unequal variances rejected H_0 of equal Arctic mean SAT anomalies between 927–1026 CE and 1903–2002 CE for 93% ensemble members. However, when considering hypotheses with a one-tailed test 400 no conclusive answer can be reached. Although the MCA appears slightly warmer on a centennial time-scale compared with the last 100 years as shown in Figure 2a, testing rejects H_0 for 64% of the ensemble members only, whereas for the opposite alternative hypothesis (i.e. 1903-2002 CE warmer than MCA on average) the H_0 rejection rate is as high as 29%.

Though this result somewhat favors the alternative hypothesis of $\overline{SAT}_{MCA} > \overline{SAT}_{CWP}$ the difference in the rejection rates appears negligible. We conclude therefore that given the collection of the proxy and instrumental data, and the reconstruction

405 technique used, it is not possible to infer whether the Arctic summers of the last 100 years of the reconstruction (i.e. before 2002 CE) were unprecedentedly warm when compared with the previous major warm climate anomaly back to 750 CE. We note also that higher variability in the derived ensemble of realisations for the mean Arctic SAT anomaly during the warmest decade-long intervals of the MCA and CWP similarly prevents from reaching any firm inference on the relative magnitudes of the two decade-long anomalously warm periods of the new reconstruction.

410 **4.3 Spatial signature of past and recent extreme temperature anomalies**

The distribution of extremely warm and cold years in both space and time is analysed by ranking the years according to their seasonal temperature for each ensemble member and the reconstruction node. Due to insufficient proxy data density and hence the inflated intra-ensemble variance (see Figure A2) in the early part of the reconstruction period, the analysis is limited to the time after 750 CE. For the Arctic average the probability density for each year to be ranked as warmest or
415 coldest is calculated across the entire ensemble using the spatial mean SAT. To check the statistical significance of the derived probability densities, the analysis is replicated on an ensemble of surrogates derived from the original reconstruction ensemble using block bootstrapping of the spatial mean reconstructions along the time axis. The block size of 10 years was assigned using an ensemble average first order autocorrelation coefficient of 0.8 and Mitchell et al. (1966) formula with adjustment of Nychka et al. (2000), yielding the efficient number of degrees of freedom in the data of about 125. The derived time-average
420 0.975 percentile of the probability density for the bootstrap surrogates is then used as the respective quantile for marking the years as potentially coldest or warmest during the analysis period (Figure 8). In order to highlight a decadal scale variability in occurrence of warm and cold extremes, the fractions of potentially warmest/coldest years per decade are calculated in sliding 10-year long windows. In order to reduce the effects of the reconstruction uncertainties, the reconstruction is averaged over five degree longitudinal bins. To take the spatio-temporal autocorrelation into account during significance testing, the bootstrap
425 replicates are drawn as 10-year long time slices from individual reconstruction ensemble members. The analysis results are presented as a time–longitude colour map in Figure 9a.

The results of the analysis are reflective of the longer term (millennial and secular) pan-Arctic tendencies in the seasonal SAT, yet the inter-regional differences are made clear as well. Of the series of past and present exceptional warmings, compared with the part of the present-day warm period before 2002 CE, the peak of the MCA features the two phases of a pronounced
430 pan-Arctic warming with a consecutive series of spatially coherent warm extremes between ca. 920–970, CE (Figure 9b). On decadal time-scale (Figure 9a) the MCA is marked over the whole region by anomalies having a persistent high fraction of likely warmest decades with no decades containing a year ranked as coldest.

In particular, seven out of ten years during the decade of 926–935 CE making the first MCA sequence of warm extremes and six out of ten years of 954–965 CE making the second maximum were ranked as statistically significant warm extremes
435 among the ensemble members. This agrees with a previously found reconstruction decadal scale temperature maximum since at least 750 CE for the first of the two periods. Note that sequences of potentially warmest years and hence decades with a higher fraction of extremes are also detected before 800 CE, though the 8th century does not appear in the reconstruction as particularly warm on average.

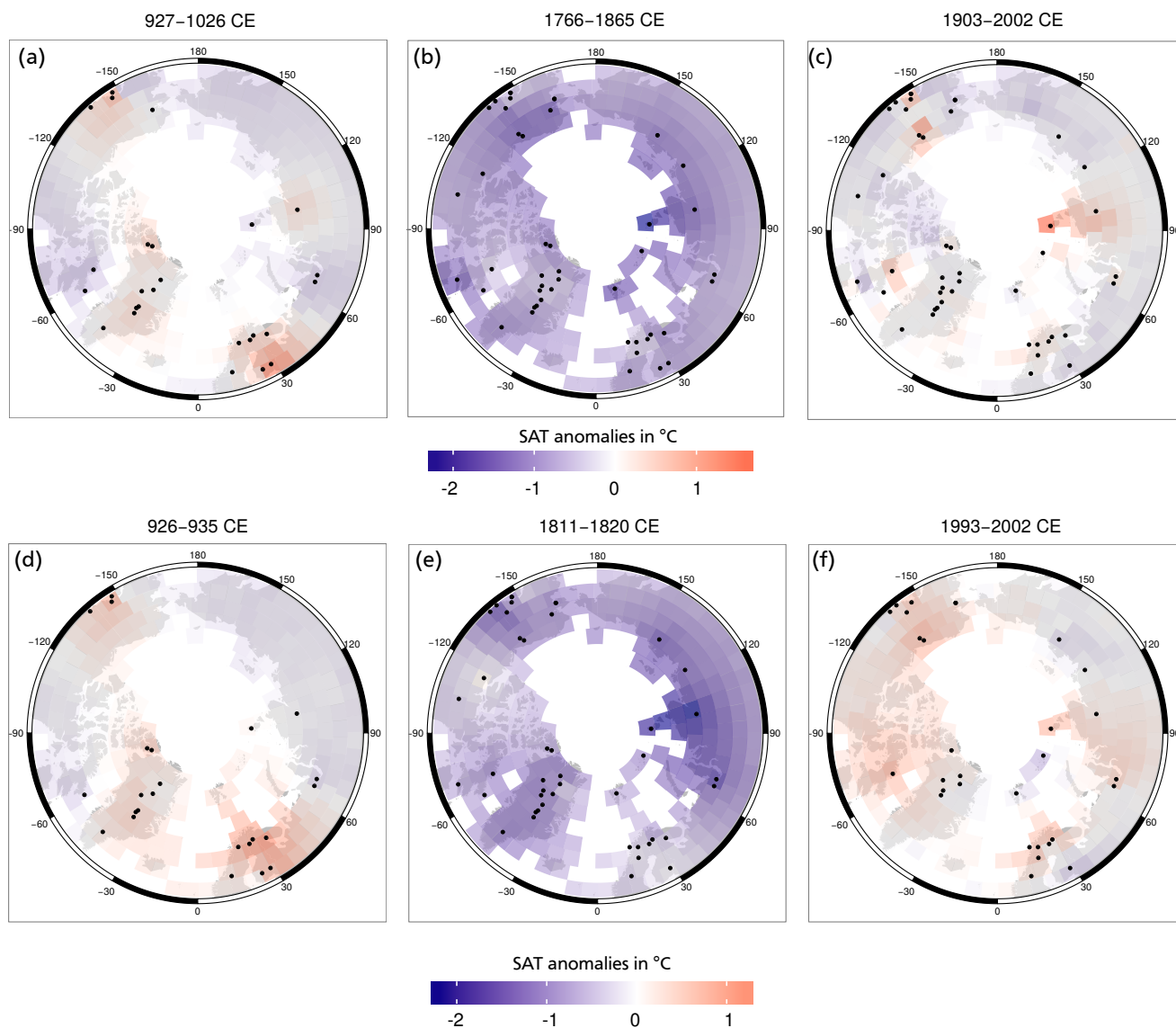


Figure 7. Ensemble average of the reconstructed Arctic2k SAT anomalies over the century-long periods of (a) 927–1026 CE, (b) 1766–1865 CE and (c) 1903–2002 CE; (d) Ensemble average SAT anomaly over the period of 926–935 CE, a potentially warmest decade since 750 CE with seven of ten years top ranked as potentially warmest; (e) Ensemble average SAT over the period of 1811–1820 CE, a potentially coldest decade since 750 CE with seven out of ten years ranked potentially coldest; (f) Ensemble average SAT anomaly over the period of 1993–2002 CE, a potentially warmest decade after the MCA with 5 out of 10 years ranked as potentially warmest. Colours show the temperature anomalies. Proxies marked by black dots.

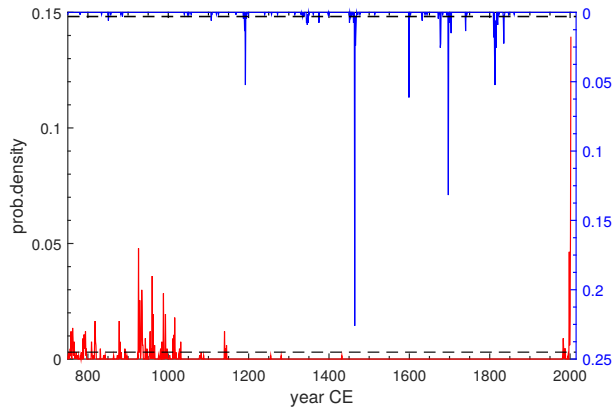


Figure 8. Probability density of statistically significant, potentially warmest (red) and coldest (blue) years over the the period 750-2002 CE. Dashed lines indicate the 95% significance level estimated from the ensemble of bootstrap surrogates.

Figure 9b also highlights a difference in time evolution of the regional expression of the MCA via the spatial incoherence
 440 of extremely warm years/decades this overall warm period. A somewhat earlier onset of warming in the European to Asian
 domain is evident from an increased frequency of warm extremes east of zero meridian around 920 CE, followed by a coherent
 warming in the Greenland and North Atlantic (NA) sector of the study domain. Figure 9b also suggests that a second phase
 of the MCA could mainly be localized west of the prime meridian. Figure 7d exemplifies a picture of a pan-Arctic warming
 during the first warm decade 926–935 CE of the first phase of the MCA with the largest reconstructed positive anomalies
 445 attained within the 170° W–30° E domain and 7 of 10 years ranked as potentially warmest in the reconstruction ensemble.
 A sequence of less pronounced MCA warm extremes occurred between 980-1040 CE localized primarily within the Atlantic
 sector (Greenland/Europe) of the study domain and do not exhibit as clear temporal coherence as the two main phases of the
 MCA.

Figures 8 and A2 and demonstrate that the period after the MCA termination features a variable climate as manifested by an
 450 alternating sequence of potentially warmest and coldest years detected on the regional scale. Yet there is a pronounced lack of
 the pan-Arctic warm extremes, with a short exception of a 15-year long warmth centered at 1142 CE. The following transition
 into the cold LIA is clearly marked by a drop in the frequency of potentially warmest years/decades to zero. During the LIA the
 cold extremes dominate on both the regional (Figure 9b) and pan-Arctic scales (Figure A2) until the onset of the contemporary
 warming after ca. 1880 CE. The first potentially warmest year after the termination of the MCA is detected only in 1983 CE.

455 One can discern five major clusters of cold extremes during the LIA with one of the years of 1192, 1464, 1599, 1697 and
 1813 CE ranked coldest in the majority (52%) of reconstruction ensemble members. Figure 9 suggests that 1464 CE is most
 likely to be the coldest year after 750 CE, while the coldest decade of the reconstruction is represented by a sequence of
 spatially coherent potentially coldest years within 65° W–180° E (Figure 9b). Figure 7e shows the spatial pattern of cooling

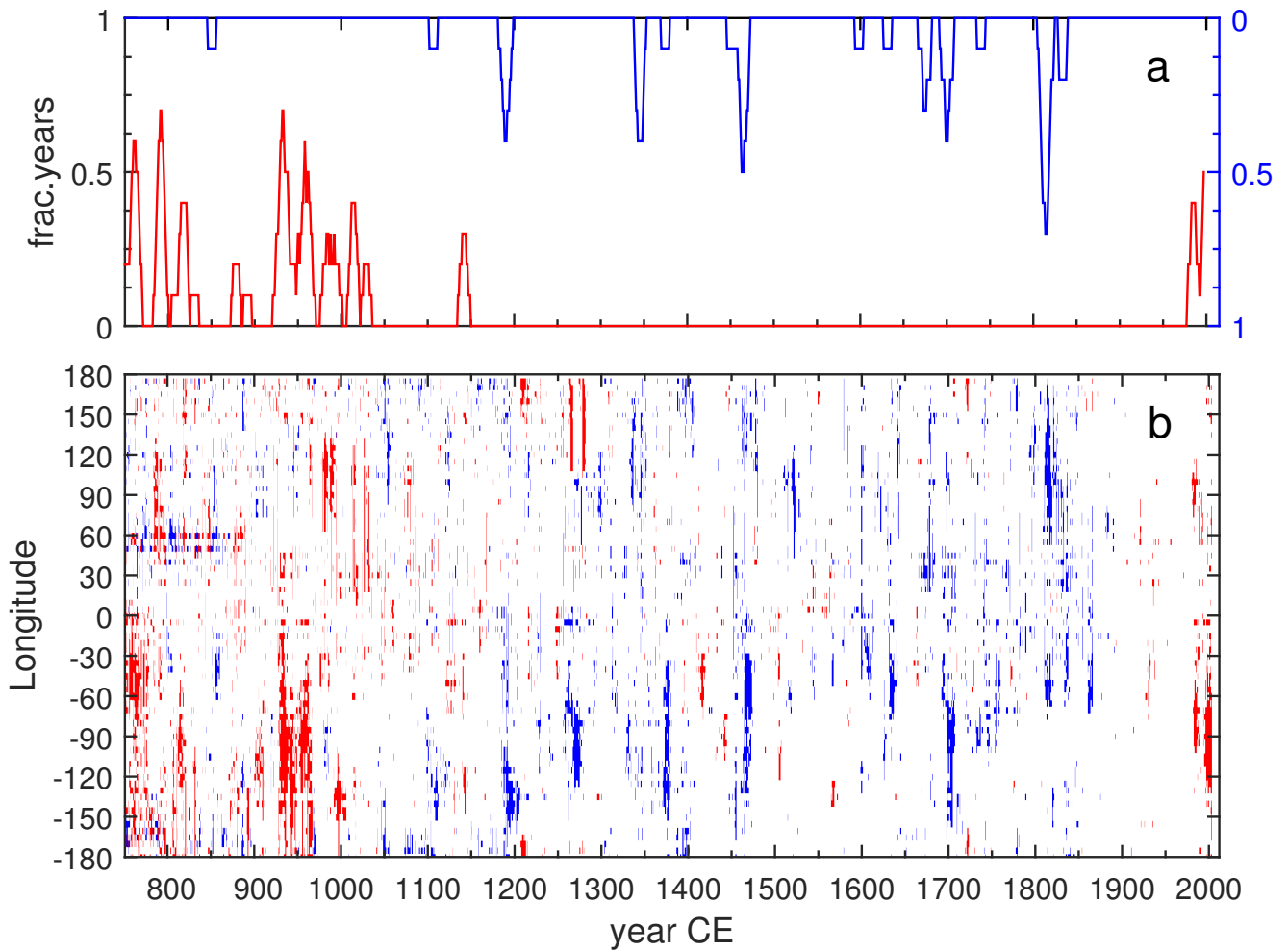


Figure 9. (a) Fraction of potentially warmest/coldest years per decade with respect to time. (b) Occurrence of statistically significant, potentially warmest (red) and coldest (blue) years over the period 750-2002 CE in different sectors of the Arctic domain.

for this decade of the LIA with seven out of ten years over the period of 1811–1820 CE, ranked potentially coldest across the
460 entire reconstruction ensemble.

Contemporary warming is manifested as a sequence of potentially warmest years starting in 1980 CE within 45–100° E
and 60–110° W and since 1995 propagating to almost the entire reconstruction domain. Figure 7f shows a spatial map of
temperature anomalies for the period 1993–2002 CE, that features 5 out of 10 statistically significant warm extremes on the
pan-Arctic scale. When compared with the probability density marginalised over the spatial domain displayed in Figure 8,
465 contemporary warming clearly reveals a coherence both in the spatial domain and agreement over the range of ensemble
members that is at least as strong as the estimates made for the MCA. Additionally, about 30% of the potentially warmest years
in the entire reconstruction ensemble were registered in the time interval of 1993–2002 CE. The year 2002 is ranked warmest
in 14% of the reconstruction members which is almost three times as many as any other potentially warmest year detected
in the analysis. One should emphasise that this statistically significant sequence of warm extremes was detected outside the
470 calibration period, which provides another indirect proof for a skill of our new Arctic reconstruction. This reconstruction,
however, does not extend into the very last 15 years, over which warming in the Arctic has been continuing. With these years
included in the analysis, the signature of the CWP would much likely become more prominent (see discussion in Section 4.1).
The warmest periods in the reconstruction shown in Fig. 7 share similar features in the higher latitudes. The circum-Arctic
warm anomalies at the shorelines are linked in the current period to the receding sea ice margin. This is indicative of a possible
475 minimum of sea ice extent similar to the one observed now during the MCA.

5 Discussion and conclusions

This paper presented a new circum Arctic CF reconstruction of summer season temperatures back to 750 CE with the Arctic
average SAT anomaly extended back to 1 CE. The reconstruction uses a subset of 54 annually resolved temperature sensitive
terrestrial proxy archives of various types mainly from an updated and corrected PAGES2k database supplemented with 6 new
480 recently published Greenland ice core series.

The technique applied is a recent extension of the Bayesian BARCAST which explicitly treats climate archives with dating
uncertainties which previously would be used on their “best guess” chronologies. Another added value of using the Bayesian
technique was a generation of the ensemble of 670 equally likely, independent realisations of past CF evolution that enabled
us considering the past climate regional variability in a probabilistic framework. Therefore this new Arctic2k reconstruction is
485 essentially an ensemble of possible realisations of the past Arctic summer temperatures given the data and the reconstruction
technique used.

The quality of the reconstruction in the spatial and temporal domains was tested using a suite of metrics such as continuously
ranked probability score ($\overline{\text{CRPS}}_{\text{pot}}$) and the Reliability score which are more appropriate for the Bayesian framework than
the “Coefficient of Efficiency” and “Reduction of Error”, which are typically used in palaeoclimate research. Judging from
490 these scores it could be demonstrated that the new reconstruction is skillful for the majority of the terrestrial nodes in the
reconstruction domain, making it a useful product for studying the late Holocene Arctic temperature variability at regional

scales. However, from the analysis of intra-ensemble variability, but also from analyses on the extreme years and the calculated confidence intervals the reduction of skill back in time is apparent. This is mostly caused by the proxy network, which is getting sparser when going back in time, and should be taken into account when the new reconstruction is used for making any quantitative inferences.

Although this study is mainly focused on presenting the new reconstruction and assessing its quality, we also ran some basic quantitative data analysis in order to uncover the potential of the new product and consider the results in light of previous studies on the subject. In particular, it is demonstrated that the area averaged Arctic2k reconstruction features similar major cold and warm periods throughout the last two millennia and thus compares favourably with earlier studies targeting a similar season and region.

The major findings from the analysis of the new reconstruction are as follows:

There is a pronounced orbital scale cooling trend over the Common Era – a period over which the summer insolation has mostly been decreasing, although the spatial pattern cannot be reliably reconstructed over the full Common Era due to the sparse proxy network before ca. 750 CE. Since the proxy dataset from Greenland is dominated by oxygen isotopes series from ice cores, these can be subject to a possible warm bias during the LIA bias caused by increased storm activity (Fischer et al., 1998) and/or be influenced by the site and source temperature compensating effects (Hoffmann et al., 2001; Masson-Delmotte et al., 2005). The ice cores from northern Greenland are also expected to have a higher fraction of summer precipitation than those from the south due to the effect of continentality on the annual accumulation, and hence exhibit a higher sensitivity to summer conditions. While site and source temperature compensating effects for the individual series can be accounted for by using the records of deuterium excess (Masson-Delmotte et al., 2005), other potential biases are difficult to resolve without additional support, e.g. from general circulation models.

The analysis of the reconstruction reveals the spatial signatures of the two major climate anomalies back to 750 CE, the MCA and LIA, as well as the beginning of the CWP in the circum-Arctic region. Although there is evidence for prominent and lasting temperature fluctuations in the pre-750 CE period as well, these results should be interpreted cautiously due to the drastic reduction in proxy data density in the early part of the reconstruction period. The MCA in the circum-Arctic region can be associated with a century-scale period between ca. 920–1060 CE showing an area average SAT anomaly of $0.1 \pm 0.1^\circ\text{C}$. The MCA features two temperature maxima, both showing similar spatial extent of the regional SAT anomalies with largest expression in the North American segment of the Arctic realm. A coherent warming of the period 927–936 CE during the first maximum of the MCA is associated with a potentially warmest decade of the reconstruction with the area average summer temperature anomaly of $0.48 \pm 0.31^\circ\text{C}$. While the most recent warming shows an even stronger regional coherence than the MCA, even across continents (PAGES 2k Consortium, 2013; Ljungqvist et al., 2016), the MCA was still an unusual and extremely warm period in the context of the past two millennia. However, given the input data available and the reconstruction method used it cannot be decided with any statistical significance whether the MCA or the CWP was warmest in the reconstruction.

The new reconstruction suggests a relatively long, though interrupted by abrupt decadal-scale warmings, transition to the LIA after the second of the two MCA maxima ends at around 1060 CE. The coldest century-long period of 1766–1865 CE

shows an almost spatially coherent circum-Arctic summer cooling. The cooling over the LIA, from essentially around the late 11th century went on until the mid 19th century CE. Most of the Arctic was coldest during the decade of 1811-1820 CE following the 1809 (unknown) and 1815 (Tambora) eruptions, which caused the “Year without a Summer” in 1816 over most of Europe and yielding a circum-Arctic SAT anomaly of $-0.8 \pm 0.2^{\circ}\text{C}$.

The spectral characteristics of both proxies and reconstruction show that work is still needed on generating more and longer high-quality proxy series in parallel with a reanalysis of the existing data. Especially updating many of the only half a century long North American tree ring series towards the present, but also possibly extending some of them into the first millennium CE seem to us like worthwhile efforts (Babst et al., 2017). Additionally, a relative “flatness” of spectra on sub-decadal to multi-decadal time-scales contrasting with an inflated variance of the multi-decadal to millennial variability (Appendix C) for some of the tree-ring chronologies, suggests that a reassessment and potentially a revision of the raw data processing techniques used for this chronologies would be highly desirable.

BARCAST as a CF reconstruction technique still offers a large potential for future development and use in new improved reconstructions. In addition to including explicitly the annually dated proxies with the chronological uncertainties into the scheme, what became a major innovation of the presented reconstruction, the next natural step will be a development of a theoretical and numerical framework to extend the technique to non-annually dated proxy archives with chronological uncertainties. This will enable a substantial extension in the proxy coverage both in the spatial and time domains including the marine realm dominated by non-annually resolved marine sediment proxy archives, potentially promoting an improved performance of the reconstructions at the low-frequency (centennial) time-scales. While relatively flexible, the BARCAST framework would however still need major modifications that allow proxy response functions that are sensitive over different frequency bands. Additionally, these frequency bands need to be either proposed and fixed a priori, with possibly insufficient information available, or determined by the algorithm itself, potentially leading either to overfitting or convergence problems.

Acknowledgements. J.P.W. gratefully acknowledges support from the Centre for Climate Dynamics (SKD) at the Bjerknes Centre. D.V.D. contribution to the Arctic2k was partly supported by Tromsø Research Foundation via the UiT project A33020. D.V.D., T.N. and J.P.W. also acknowledge the IS-DAAD project 255778 HOLCLIM for providing travel support. F.C.L. is partly supported by a grant from the Royal Swedish Academy of Letters, History and Antiquities and the Bank of Sweden Tercentenary Foundation (*Stiftelsen Riksbankens Jubileumsfond*). T.N. was supported by the Norwegian Research Council (KLIMAFORSK program) under grant no. 229754. PF is supported by an NSERC-discovery grant number RGPIN-2014-05810.

This is a contribution from the interdisciplinary and international framework of the Past Global Changes (PAGES) 2k initiative (Arctic2k), which in turn received support from the U.S. and Swiss National Science Foundations.

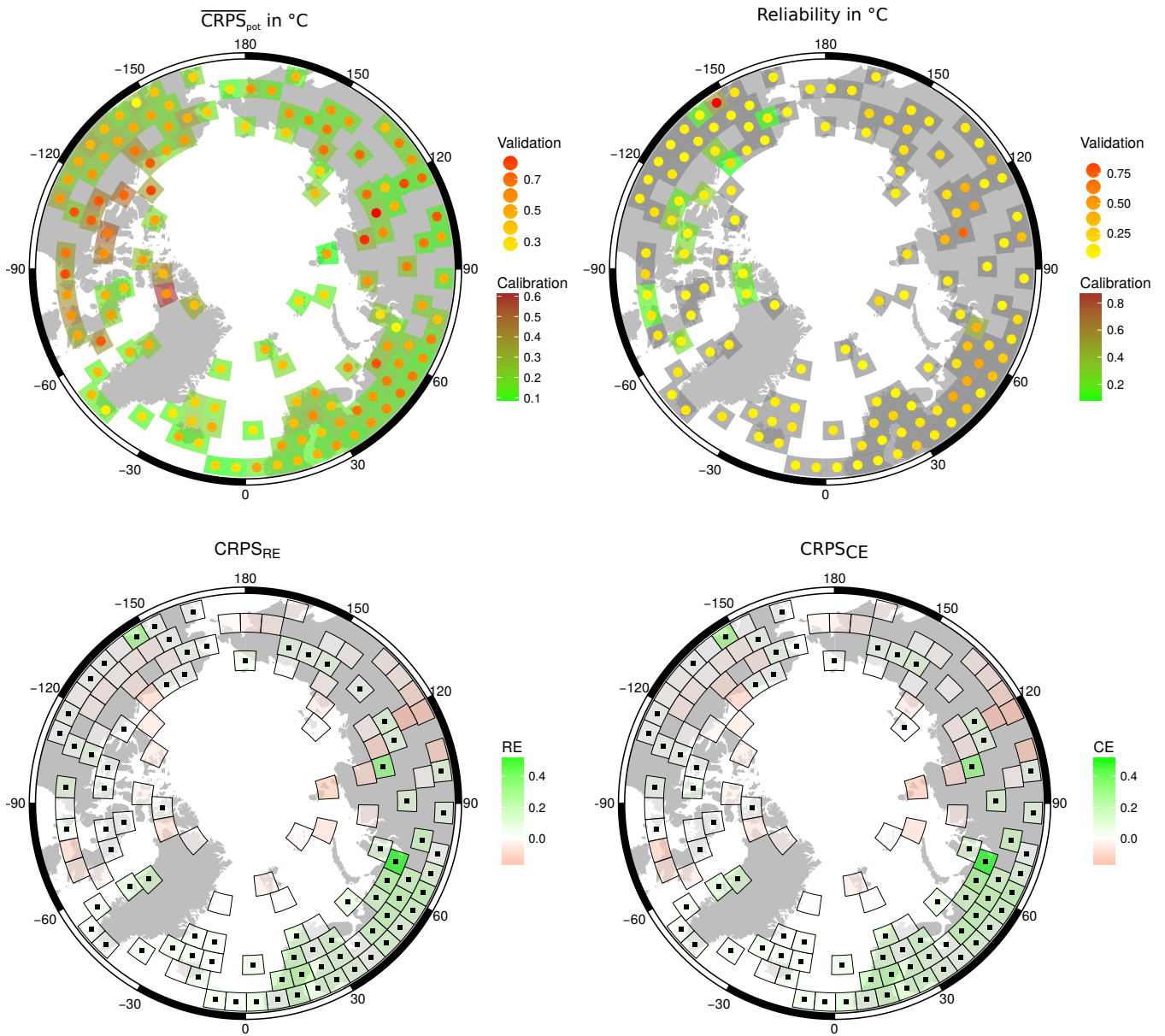


Figure A1. Calibration and Validation results. Top row: $\overline{\text{CRPS}}_{\text{pot}}$ and Reliability score for the calibration (quadrilaterals) and validation (points) period. Bottom row: CRPS scores corresponding to an ensemble-based version of the reduction of error (RE) and coefficient of efficiency (CE) estimates. Squares denote grid cells with positive CRPS-RE or CRPS-CE, indicating a skilful reconstruction in the validation period. Grid cells with few data in the validation period show a lack of skill, which might be an artifact.

Appendix A: Calibration and Validations Statistics

In order to estimate the skill of the reconstruction two different measures are used, the average potential continuously ranked probability score ($\overline{\text{CRPS}}_{\text{pot}}$) and the reliability (Reli) score (Hersbach, 2000; Gneiting and Raftery, 2007; Werner and Tingley, 2015; Tipton et al., 2016). The reliability analyses the accuracy of the uncertainty estimates. In principle it compares the empirical coverage rates of uncertainty bands with their respective nominal coverage rate, e.g. a 95% confidence band should contain the target truth in 95% of the time. The $\overline{\text{CRPS}}_{\text{pot}}$ measures the accuracy of the reconstruction itself, i.e. the mismatch between the best estimate and the target. In a deterministic reconstruction it is equal to the mean absolute error. Both measures retain the original units of the data, and both signal a better result the lower they are. The results are shown in Figure A1 (top row). For the calibration (validation) interval, the $\overline{\text{CRPS}}_{\text{pot}}$ is mostly below 0.2°C (0.5°C), and the Reliability is sharper than 0.1°C. This in principle indicates a relatively low reconstruction error, with uncertainty bands that (within reason) reflect the correct uncertainties.

Additionally the skill of the reconstruction beyond forecasting the calibration or validation period climatology is evaluated. In palaeoclimate reconstructions this is often assessed by the Coefficient of Efficiency and the Reduction of Error statistics (Cook et al., 1994). These analyse whether the reconstruction is closer to the validation target than the climatological mean of the calibration or validation period respectively. However, these are not proper scoring rules (Gneiting and Raftery, 2007) and should thus not be used analysing the results of a probabilistic reconstruction method. In essence, these two skill measures compare the reconstruction over the validation period to the mean climatology of the calibration (RE) and validation (CE) period (Lorenz, 1956; Briffa et al., 1988).

As introduced by Tipton et al. (2016), in order to generate a similar statistic, the mean and standard deviation over the validation and calibration intervals for each location with instrumental data are calculated. These are then used to generate an ensemble of timeseries. These act as simple surrogates for the calibration and validation interval climatology. These are then compared against the target instrumental data of the validation period, using the $\overline{\text{CRPS}}_{\text{pot}}$. Should this value be lower than the $\overline{\text{CRPS}}_{\text{pot}}$ comparing the actual reconstruction ensemble against the instrumental data, the reconstruction does not add skill over the climatology. Thus, subtracting the $\overline{\text{CRPS}}_{\text{pot}}$ of the reconstruction from the $\overline{\text{CRPS}}_{\text{pot}}$ of the surrogates results in measures that indicate a skilful reconstruction if they are positive, i.e. a reconstruction that performs better than the climatology over the calibration (validation) interval. We denote these two scores as CRPS_{RE} and CRPS_{CE} . Figure A1 bottom row shows that about half of the grid cells with instrumental data have a CRPS_{RE} and CRPS_{CE} that is above zero – and these grid cells are mostly those that have the longest instrumental time series (inside and outside the calibration interval). Thus, these results not only reflect a possibly weak reconstruction but more likely the lack of actual instrumental data to construct any meaningful comparison statistics over the validation period.

Appendix B: Intra-ensemble variance of the reconstruction

Figure A2 presents the time changes in the spatially averaged intra-ensemble variance as a measure of the spread across the ensemble members. The variance shows a progressive decline over the pre-industrial reconstruction more pronounced in the

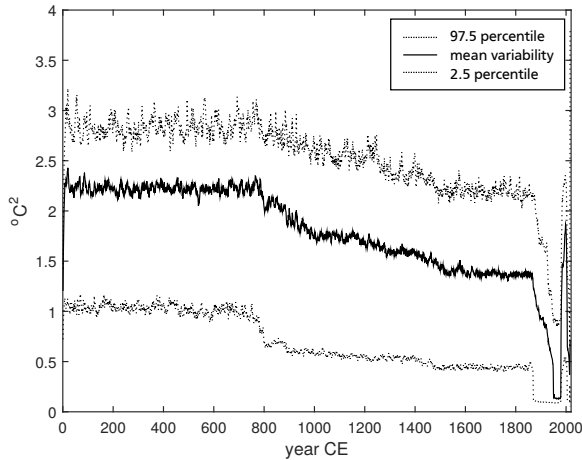


Figure A2. Time variability of spatially averaged intra-ensemble variance of the Arctic2k reconstruction together with the respective ensemble-based 95% CIs.

confidence intervals (CIs) for the period 800–1000 CE (which is linked with the time of an expansion of the multi-proxy
 590 network). Along with the intra-ensemble variability, a progressive increase in the proxy data density over time contributes to the observed decrease in the ensemble spread. The introduction of the instrumental data into the scheme (corresponding to a calibration period in the regular climate reconstruction language) causes a sharp drop in the spread after 1850 CE that reaches a minimum around 1950 CE, a period of the maximal instrumental data coverage. Figure A3 further illustrates the effects of the spatial changes in input data density on the reconstruction intra-ensemble spread. The figure presents intra-ensemble spatial
 595 variances averaged over four time periods. The selected time-slices are associated with periods of distinctly different proxy and calibration data density: part of the Roman Warm Period 200–300 CE with a CF reconstruction based on 8 proxy records only, one of the coldest period of the LIA 1600–1700 CE with a complete multi-proxy network, and parts of the calibration period of 1850–1900 CE and 1950–1980 CE, representative of the low and high instrumental data coverage, respectively.

Appendix C: Statistical properties of the reconstruction and Input Data

600 As an additional test for the reliability of the proxy series and the validity of the climate field reconstruction, the temporal persistence of both need to be analysed. The Kolmogorov-Smirnov test is first used to test the normality of the proxy records and the climate field reconstruction, with a significance level $p = 0.05$, and additionally Q-Q plots are checked. Then, the power spectral density (PSD) is used to study the variability on different frequencies for the records, using the periodogram as an estimator of the PSD. The periodogram is defined here in terms of the discrete Fourier transform H_m as $S(f_m) = (2/N)|H_m|^2$,
 605 $m = 1, 2, \dots, N/2$. The sampling time is the time unit (here: years), and the frequency is measured in cycles per time unit:

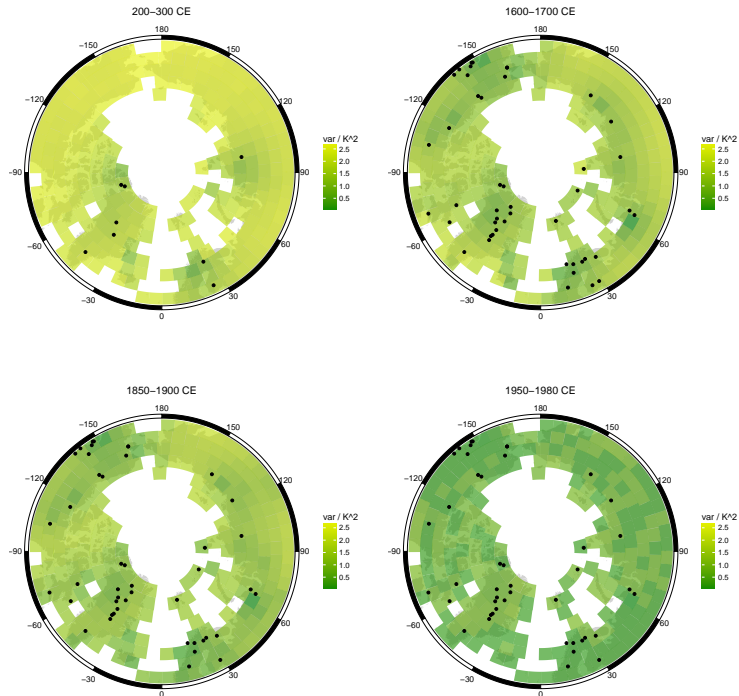


Figure A3. Time averaged intra-ensemble variance of the Arctic2k reconstruction shown for the four subperiods with a distinct difference in proxy data density (200–300 CE vs. 1600–1700 CE, panels a and b) and calibration subperiods with different instrumental data coverage (1850–1900 vs. 1950–1980 CE, panels c and d). Black dots shows the proxy locations with a least one data point over the period of averaging.

$f_m = m/N$. $\Delta f = 1/N$ is the frequency resolution and the smallest frequency which can be represented in the spectrum, while $f_{N/2} = 1/2$ is the Nyquist frequency.

The characteristic shape of the spectrum provides useful information about the temporal persistence or memory of the underlying process. If the data is close to Gaussian and monofractal, the second order statistics are sufficient to describe the statistical properties of the data. The spectral shape can then be associated with well-known stochastic processes. If the spectrum has a power-law shape, the process exhibits long-range memory (LRM). The strength of memory in an LRM stochastic process is described by the spectral exponent β , which can be estimated by a linear fit to the power spectrum; $\log S(f) = -\beta \log f + c$. If the spectrum is Lorentzian (power law on high frequencies, flat on low frequencies), the underlying process is closer to an AR(1) process. In all spectral analyses, the fitting is applied to log-binned periodograms to ensure that all time scales are weighted equally. If the Gaussianity and monofractality criteria are not met, there could be underlying structures such as intermittency that are not captured by the analyses. In the temperature time series considered here, deviations from normality are due to nonlinear dynamics associated with e.g. volcanic eruptions.

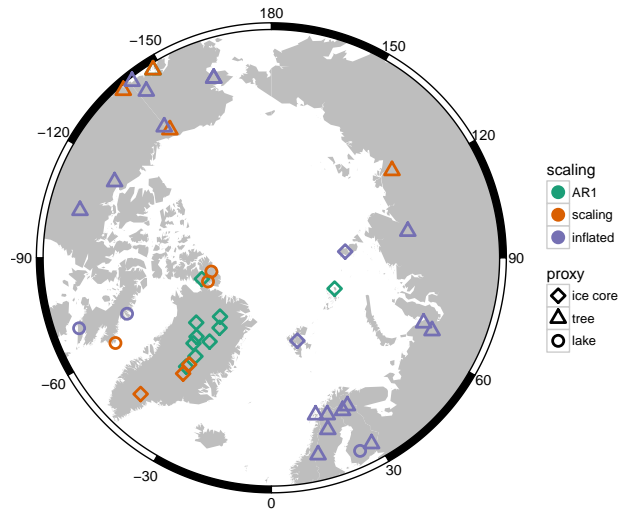


Figure A4. Proxy type (triangles: ice cores, diamonds: tree rings, squares: lake sediments,) and persistence properties colour coded.

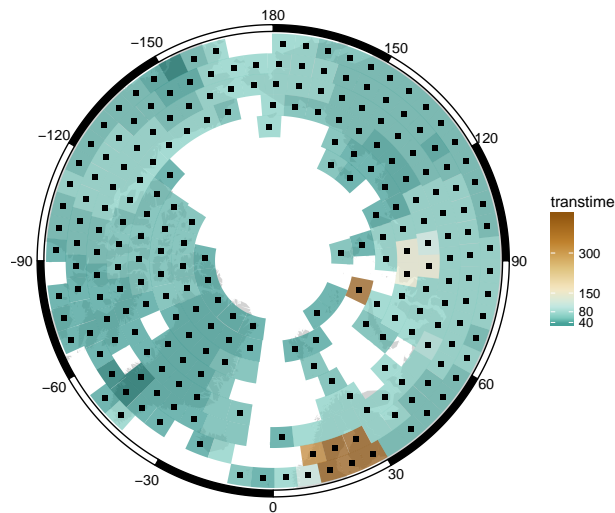


Figure A5. Analysis of scaling properties of the reconstruction. The transition time-scale (colour coded) and strength of change (black dot: exponent change > 1). Most of the reconstruction domain resembles an AR 1 process.

C1 Spectral analyses of the proxy records

The six proxy records originating from lake sediments deviate substantially from a Gaussian distribution and thus had to be normalized before analysis. After normalization, around 60% of the individual proxy records are Gaussian according to the Q-Q plots and the p-values from the Kolmogorov-Smirnov's test. The characteristic shape of the spectra for all of the proxy records are classified into three spectral categories: (1) AR(1) processes, (2) persistent power-law processes with spectral exponent $0 < \beta < 1$, and (3) records exhibiting weak persistence on high frequencies, and increased levels of variability on frequencies corresponding to time scales longer than decadal–centennial. Figure A4 illustrates the spatial distribution of the proxy records with proxy type indicated by shape, and categories with colours. The Greenland records are similar to either an AR(1) or an LRM process. The Greenland LRM records are in fact only weakly persistent, with a spectral exponent $0 < \beta < 0.3$. There is thus little evidence of long-term cooling due to orbital forcing from these records. Along with a few tree-ring records, the Greenland ice core records are the longest records used for the present reconstruction. As the low frequency variability of these records dominates the reconstructed long-term variability, the resulting reconstructions does exhibit similarly low variability at long time scales.

The proxies of category 3 are mainly tree-ring records, widely distributed along the reconstruction region. These records may require additional attention in future studies, as the level of high versus low frequency variability is unusual compared to other proxy records and also instrumental measurements. Similar spectral characteristics were obtained for other tree-ring chronologies in (Franke et al., 2013; Zhang et al., 2015; Esper et al., 2015; Büntgen et al., 2015). The persistence in a number of millennium-long climate model simulations and proxy-based temperature reconstructions have been studied in (Østvang et al., 2014; Nilsen et al., 2016) using the power spectrum along with selected other techniques. In these studies, LRM was detected in all records up to centennial/millennial time scales.

C2 Spectral analyses of climate field reconstruction

The resulting p-values from Kolmogorov-Smirnov's test indicate that for individual locations of the field reconstruction, about 60-80% of the ensemble members are Gaussian. For each ensemble member of the reconstruction, and each location, a spectral analysis is performed. Then, the persistence is analysed for ensemble-averaged spectra of each location. The analyses indicate that the reconstructed temperature is best described as an AR(1) process in time at almost all grid cells. This is not surprising, as the longest proxy records exhibit low levels of long-term variability, and the BARCAST reconstruction technique assumes an AR(1) model for the temporal evolution of the temperature. Further details about the characteristic transition times are obtained by making a least-squares fit of a bilinear continuous function for the spectrum. The detected break is located where the two lines intersect. The coloured map in Figure A5 shows the spatial distribution of the found transition time scales, black dots indicate that the difference between the spectral exponents for low and high frequencies is more than one. The spatial coherence indicates that BARCAST performs well when extrapolating temperatures to locations where observations are unavailable. For most of the area we find a marked transition in the spectral slope (black symbols). Only the East coast of Greenland and the Scandinavian sector has slightly less difference between the high- and low-frequency variability, that

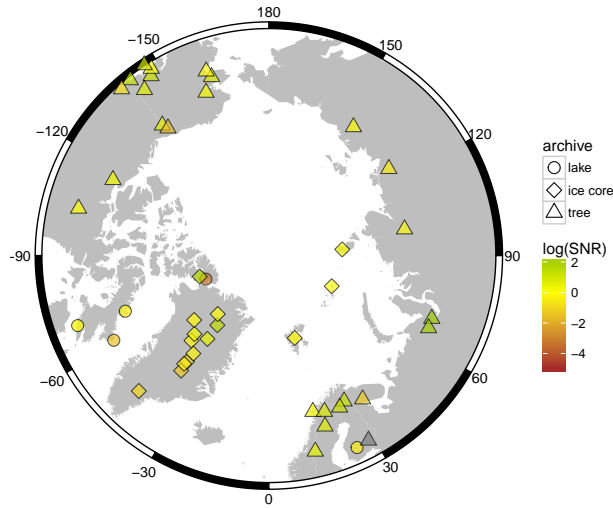


Figure A6. The mean of the posterior SNR for all proxy series. Note the logarithmic scale. There is one series with a negative β_1 (grey).

is, the spectral exponent does not change much between the two identified scaling regimes. This indicates more similarity to an LRM process. Additionally, the transition time scale is above a hundred years for a number of single locations. There, the reconstruction is indeed closer to an LRM process than an AR(1) process.

C3 Proxy response

655 The BARCAST output parameters contain information on the proxy signal strength (β_1 in Eq. 1b) and proxy noise level (τ_P^2 , Eq. 1b). Under the assumption of a unit standard deviation climate variable, the ratio of β_1/τ_P returns an estimate of the Signal to Noise Ratio (SNR, in amplitudes) of the individual proxy series. The mean of all ensemble draws is shown in Fig. A6. Note that one proxy series (Finnish Lakelands) has a negative (inverted) response ($\beta_1 \approx -0.38 \pm 0.7$).

660 In general, most tree ring series have a SNR > 1, and they seem to be the highest quality proxies on average, followed by the ice core data. The lake sediments add only some skill, but are important especially in regions with no other data present, such as Eastern North America. This might be caused by the in general higher dating uncertainties (see discussion in Werner and Tingley, 2015) or a response on different time scales. This underlines the necessity to really use multiple proxies, and to further improve the reconstruction methods to make use of information on different time scales.

Appendix D: Input proxy data

665 D1 Time-scale modelling

In order to account for possible chronological uncertainties in the annually resolved proxy records, the technique of Comboul et al. (2014) is applied to the proxies with layer counted time-scales in for the generation of ensembles of chronologies. BAM (Banded Archive Modelling) simulates the time-scale counting procedure as a superposition of two cumulative Poisson processes with age perturbations associated with two categories of errors either miss (type 1) or double-count (type 2) of an annual layer. More specifically, for each measurement x_i assigned a time t_i with $i \in \{1, \dots, n\}$, and a neighbouring x_{i+1} with t_{i+1} , $i \in \{2, \dots, m\}$, the vector of time increments δ , $t_{i+1} - t_i = \delta_i$ comprises two independent stochastic processes P^{Θ_1} and P^{Θ_2} , with parameters Θ_1 and Θ_2 , representing the rates of missing and doubly counted annual layers, respectively. We note that the approach implicitly assumes the independence of the two stochastic processes and depth(time) invariance of the error rates.

675 For the proxy series with chronologies constructed using a combination of annual layer counting and time markers (tie points) t_k , $k \in \{1, \dots, K\}$, such as volcanic sulphate peaks or tephras with ages known to a specific precision (σ_k), a two-step procedure was implemented. The first step involved an MCMC simulation of M perturbed sets of tie points $[t_k^{\tilde{m}}]$ following Divine et al. (2012), where $[\bullet]$ stands for rounding the argument to the nearest integer. For each particular set m of perturbed tie points and a time interval $[t_k^{\tilde{m}}, t_{k+1}^{\tilde{m}}]$, $k \in \{1, \dots, K-1\}$ between the perturbed pairs of tie points time-scale modelling was applied, and only those that satisfied a criterion of $\sum \delta_i = t_k^{\tilde{m}} + 1 - t_{k+1}^{\tilde{m}}$ were retained for further analysis. For ages older than $t_K^{\tilde{m}}$ a model with a free boundary was used instead. In total $M = 1000$ time-scales \tilde{t}_i^m per proxy archive were generated. Using interpolation, the proxy series x_i were further projected on the generated time-scales \tilde{t}_i^m to yield the ensemble of proxy series with perturbed chronologies.

The error rates $\{\Theta_1, \Theta_2\}$ were estimated for each particular proxy archive. In the framework the counting procedure is defined, for each point t_i of the true unknown time-scale the uncertainty of the modelled time-scale follows the Skellam distribution with parameters $\{\lambda_1, \lambda_2\} = \{(t_s - t_i)\Theta_1, (t_s - t_i)\Theta_2\}$ where $(t_s - t_i)$ denotes the time lapse between t_i and a counting start point t_s (Comboul et al., 2014). For a symmetric error rate $\Theta_1 = \Theta_2$ and $(t_s - t_i)$ large enough, it converges to a normal distribution $N(0, \lambda_1 + \lambda_2)$. The error rates can therefore be estimated as

$$\{\hat{\Theta}_1, \hat{\Theta}_2\} = \operatorname{argmin}_{\Theta_1, \Theta_2} (\sqrt{\delta t_{\max} * (\Theta_1 + \Theta_2)} - \Delta_t / 4), \quad (\text{D1})$$

690 where for a particular proxy archive $\delta t_{\max} = \operatorname{argmax}_k (t_{k+1} - t_k)$, $k \in \{1, \dots, K-1\}$, or the entire length of the chronology, and Δ_t denotes an estimated largest offset of the reported time-scale from the unknown true time-scale. For the majority of records we estimated the type 1 and type 2 error rates using the authors reports on the tie point used and uncertainty of the constructed chronologies. For the few archives where the chronological uncertainties were not reported, a conservative estimate of $[\Theta_1, \Theta_2] [0.05, 0.05]$ was assigned.

695 Table A1 shows the list of proxy series together with parameters of the model used to simulate the annual layer counting process. In total ensembles of time-scales for 13 annually dated records of the Arctic2k network, 6 ice-core and 7 lake sediment

records, plus seven annually dated ice cores from the Greenland German traverse from 1993–1995 (recently reanalysed by Weißbach et al., 2016), are generated.

Table A1. List of the proxy records including the proxies of the Arctic2k network (PAGES 2k Consortium, 2017) with layer counted time-scales used in the present study together with parameters of the probabilistic model used in MC simulations of the layer counting process. The archives with a lacking information on the dating uncertainty are marked '*', a conservative estimate of $[\Theta_1, \Theta_2] [0.05, 0.05]$ was used in time-scale modelling.

Site ID	Pages2k site name	Location Lat, Lon	Elev., m	Proxy type	Season (month)	Time period (yr CE)	(Θ_1, Θ_2)	Reference
Arc_025	Lake Nautajärvi	61.81 24.68	104	ls	3 4 5	-555 - 1800	0.055	Ojala and Alenius (2005)
Arc_076	Soper Lake	62.92 -69.88	14	ls	6	1514 - 1992	0.01	Hughen et al. (2000)
Arc_024	Donard Lake	66.73 -61.35	500	ls	6 7 8	752 - 1992	0.05*	Moore et al. (2001)
Arc_029	Big Round Lake	69.87 -68.83	180	ls	7 8 9	971 - 2000	0.025	Thomas and Briner (2009)
Arc_020	Lake C2	82.13 -77.15	1.5	ls	6 7 8	-1 - 1987	[0.053 0.007]	Lamoureux and Bradley (1996)
Arc_004	Lower Murray Lake	81.35 -69.53	106	ls	7	-1 - 2000	0.045	Cook et al. (2009)
Arc_065	Lomonosovfonna	78.87 17.43	1250	ic	12 1 2	1598 - 1997	0.05	Divine et al. (2011)
Arc_064	ANIK	80.52 94.82	750	ic	ann	900 - 1998	0.05	Opel et al. (2013)
Arc_031	NGRIP1	75.1 -42.32	2917	ic	ann	-1 - 1995	0.0002	Vinther et al. (2010)
Arc_034	Dye-3	65.18 -43.83	2480	ic	ann	1 - 1978	0.0002	Vinther et al. (2010)
Arc_035	GRIP	72.58 -37.64	3238	ic	ann	1 - 1979	0.0002	Vinther et al. (2010)
Arc_032	Agassiz Ice Cap	80.7 -73.1	1700	ic	ann	-1 - 1972	0.0002	Vinther et al. (2010)
Arc_033	Crête	71.12 -37.32	3172	ic	ann	553 - 1973	0.0002	Vinther et al. (2010)
Arc_011	GISP2	72.10 -38.08	3200	ic	ann	818 - 1987	0.01	Grootes and Stuiver (1997)
Arc_078	Windy Dome	81.0 64.0	509	ic	ann	1225 - 1995	0.02	Kinnard et al. (2011)
16	B16	73.94 -37.63	3040	ic	ann	1469 - 1992	0.01	Weißbach et al. (2016)
17	B18	76.62 -36.40	2508	ic	ann	874 - 1992	0.002	Weißbach et al. (2016)
18	B20	78.83 -36.50	2147	ic	ann	777 - 1993	0.01	Weißbach et al. (2016)
19	B21	80.00 -41.14	2185	ic	ann	1373 - 1993	0.01	Weißbach et al. (2016)
20	B26	77.25 -49.22	2598	ic	ann	1505 - 1994	0.005	Weißbach et al. (2016)
21	B29	76.00 -43.49	2874	ic	ann	1471 - 1994	0.005	Weißbach et al. (2016)

Table A2. List of the tree ring records. Only records North of 60°N that went back at least to 1500 CE were included. This removes a number of short records, mostly from North America.

PAGES2k.ID	PAGES2k.Sitename	lat (°N)	lon (°E)	elev (m)	Time period CE	Reference	data url
NAm_091	Almond Butter Upper	65.2	-162.2	213	1406 - 2002	D'Arrigo et al. (2005)	https://www.ncdc.noaa.gov/paleo/study/3044
Arc_065	Arjeplog	66.3	18.2	800	1200 - 2010	Björklund et al. (2014)	https://www.ncdc.noaa.gov/paleo/study/3264
Arc_002	Avam-Taimyr	72	101	250	0 - 2000	Briffa et al. (2008)	https://www.ncdc.noaa.gov/paleo/study/14188
NAm_126	Coppermine River	67.2	-115.9	213	1428 - 1977	Jacoby and D'Arrigo (1989)	https://www.ncdc.noaa.gov/paleo/study/3592
Eur_013	Finnish Lakelands	62	28.325	130	760 - 2000	Helama et al. (2014)	http://www.ncdc.noaa.gov/paleo/study/16790
NAm_104	Firth River 1236	68.7	-141.6	790	1073 - 2002	Anchukaitis et al. (2013)	https://www.ncdc.noaa.gov/paleo/study/14790
Arc_074	Forfjorddalen	68.73	-15.73	200	1100 - 2007	McCarroll et al. (2013)	https://www.ncdc.noaa.gov/paleo/study/19943
Arc_007	Gulf of Alaska	61.03	-146.59	230	800 - 2010	Wiles et al. (2014)	https://www.ncdc.noaa.gov/paleo/study/19743
NAm_083	Herring Alpine	60.4	-147.8	275	1422 - 1972	PAGES 2k Consortium (2017)	https://www.ncdc.noaa.gov/paleo/study/3264
NAm_127	Hornby Cabin	64	-103.9	160	1491 - 1984	Jacoby and D'Arrigo (1989)	https://www.ncdc.noaa.gov/paleo/study/3598
Arc_016	Indigirka	69.5	147	80	1259 - 1994	Hughes et al. (1999)	https://www.ncdc.noaa.gov/paleo/study/14188
Arc_063	Jamtland, Sweden	63.24	13.34	650	783 - 2011	Zhang et al. (2016)	https://www.ncdc.noaa.gov/paleo/study/19743
	Khibiny	67.45	33.14	320	800 - 2005	McCarroll et al. (2013)	https://www.ncdc.noaa.gov/paleo/study/19943
NAm_002	Kobuk/Noatak	67.1	-159.6	100	978 - 1992	PAGES 2k Consortium (2017)	https://www.ncdc.noaa.gov/paleo/study/3706
Arc_071	Laanila	68.49	27.33	265	800 - 2005	McCarroll et al. (2013)	https://www.ncdc.noaa.gov/paleo/study/19943
NAm_032	Landslide	60.2	-138.5	800	913 - 2001	Clague et al. (2006)	https://www.ncdc.noaa.gov/paleo/study/13785
Arc_024	Lena River	70.67	125.87	180	1490 - 1994	MacDonald et al. (1998)	https://www.ncdc.noaa.gov/paleo/study/3902
NAm_088	Miners Well	60	-141.7	650	1428 - 1995	PAGES 2k Consortium (2017)	https://www.ncdc.noaa.gov/paleo/study/5244
NAm_094	Nabesna Mine	62.4	-143.1	1167	1471 - 1997	Davi (2003)	https://www.ncdc.noaa.gov/paleo/study/3605
Eur_003	Northern Scandinavia	68	25	300	-138 - 2006	Esper et al. (2012)	http://www.ncdc.noaa.gov/paleo/study/1003406
Arc_061	Polar Urals	66.9	65.6	250	891 - 2006	Schneider et al. (2015)	https://www.ncdc.noaa.gov/paleo/study/19743
NAm_003	Prince William Sound	60.5	-148.3	100	873 - 1991	Barclay et al. (1999)	https://www.ncdc.noaa.gov/paleo/study/14274
NAm_100	Seward Composite	65.2	-162.3	100	1389 - 2001	D'Arrigo et al. (2006)	https://www.ncdc.noaa.gov/paleo/study/13708
Arc_062	Tornetrask	68.26	19.6	320	-39 - 2010	Melvin et al. (2013)	https://www.ncdc.noaa.gov/paleo/study/13708 crudata.uea.ac.uk/cru/papers/melvin2012holocene/
Arc_079	Yamalia	66.8	68	30	914 - 2003	Briffa et al. (2013)	https://crudata.uea.ac.uk/cru/papers/briffa2013qsr/
Arc_008	Yukon	67.9	-140.7	300	1177 - 2000	D'Arrigo et al. (2006)	https://www.ncdc.noaa.gov/paleo/study/13758

The two largest statistically significant cooling rates in the entire ensemble with average temperature changes of $-0.05 \pm 0.01^\circ\text{C}/\text{year}$ and $-0.04 \pm 0.01^\circ\text{C}/\text{year}$ over three decades are registered at 1450 CE and 1669 CE, respectively, while a recovery after the first cooling centered at 1477 CE featured a warming rate of $0.04 \pm 0.01^\circ\text{C}/\text{year}$ over the same time period. In terms of the rate of changes attained, the first cooling/warming episode appears unique over the 2000-year long reconstruction, embracing one of the coldest decades in the reconstruction ensemble. At the highlighted centennial timescale, the most rapid changes are the MCA to LIA transition with a cooling of $-0.006 \pm 0.002^\circ\text{C}/\text{year}$ centered at 1040 CE, cooling towards one of the LIA SAT minima at 1577 CE with $-0.04 \pm 0.02^\circ\text{C}/\text{year}$, and the transition to CWP centered at 1905 CE with an average warming rate of $0.01 \pm 0.001^\circ\text{C}$ over about 30 years.

Appendix: Data availability

The input proxy data is available either through the individual publications (see tables), the majority is also available in the recent temperature database of PAGES 2k Consortium (2017) except for the NGT ice cores.

Table A3. List of the lake and ice core data from the PAGES2k database that was not used in this study.

Site ID	Pages2k site name	Location Lat, Lon	Proxy type	Time period (yr CE)	Resolution	Reason
Arc_037	Iceland	64.77,-18.37	doc	945 – 1935	30	not annual
Arc_005	Camp Century	77.17,-61.13	ic	1242 – 1967	1	20 yr averages
Arc_018	Austfonna	79.83,24.02	ic	1400 – 1998	1	interpolated onto annual scale
Arc_075	Prince-of-Wales, Ellesmere Isl.	78.4,-80.4	ic	151 – 1995	1	not annual as per original article description
Arc_044	Devon Ice Cap	75.33,-82.5	ic	1 – 1971	5	not annual
Arc_059	Renland	71.27,-26.73	ic	3 – 1983	5	not annual
Arc_045	Penny Ice Cap P96	67.25,-66.75	ic	5 – 1980	25	not annual
Arc_001	Blue Lake	68.09,-150.47	ls	730 – 2000	1	very nonlinear response, short overlap with instrumental, unclear interpretation
Arc_014	Lake Lehmilampi	63.62,29.1	ls	1 – 1800	1	exact interpretation unclear from original article
Arc_022	Hvífárvatn	64.6,-19.8	ls	-1 – 2000	1	annual and centennial signal inconsistent
Arc_069	Kongressvatnet	78.0217,13.9311	ls	232 – 2008	10	not annual
Arc_067	Hallet Lake	61.5,-146.2	ls	116 – 2005	11	not annual
Arc_050	Lake Hampitårsk	60.28,25.42	ls	1359 – 1994	14	not annual
Arc_070	Lake E	67,-50.7	ls	-3642 – 1876	19	not annual
Arc_043	Braya Sjø	67,-50.7	ls	-998 – 1999	29	not annual
Arc_040	Moose Lake	61.35,-143.6	ls	-718 – 1963	36	not annual
Arc_051	Lake Pieni-Kauro	64.28,30.12	ls	462 – 1979	44	not annual
Arc_041	Hudson Lake	61.9,-145.66	ls	-837 – 1997	47	not annual
Arc_054	Lake 4	65.1,-83.79	ls	634 – 1997	50	not annual
Arc_042	Screaming Lynx Lake	66.07,-145.4	ls	-1067 – 1988	51	not annual

Table A4. Summary of some of major features of the new Arctic2K reconstruction ensemble. Anomalies are given relative to the period of 1850–2000

Feature name	Year/Period considered, years CE	Anomaly value (STD) ^o C	Note
Warmest century	901–1000	0.00(0.13)	after 750 CE
Warmest century-long period	927–1026	0.07(0.13)	MCA
Second warmest century-long period	1903–2002	0.01(0.05)	after MCA
Warmest decade	926–935	0.48(0.31)	
Second warmest decade	1993–2002	0.41(0.28)	outside MCA, 750 CE
Coldest century	1601–1700	−0.9(0.1)	
Coldest century-long period	1766–1865	−0.94(0.09)	
Coldest decade	1811–1820	−1.5(0.2)	
Second coldest decade	1463–1472	−1.4(0.2)	
Millennial scale trend	1–1850	−0.05(0.01) ^o C/century	before the onset CWP
Largest warming trend magnitude	centered at 1905	0.01 ± 0.001	per year, centennial scale
Largest warming trend magnitude	centered at 1477	0.04 ± 0.01	per year, ca. 30 years scale
Largest cooling trend magnitude	centered at 1040	−0.006 ± 0.002	per year, centennial scale
Largest cooling trend magnitude	centered at 1450	−0.05 ± 0.01	per year, ca. 30 years scale

710 The base instrumental data (see Harris et al., 2014) can be downloaded from the BADC, the most recent version can be
reached from the CRU homepage http://browse.ceda.ac.uk/browse/badc/cru/data/cru_ts/cru_ts_3.24.01
under “observations”.

The treated input data and the R script files used for the treatment of the input data as well as the reconstruction results
(ensemble reconstruction, gridded ensemble mean and area mean), together with the program code are made available through
715 NOAA <https://www.ncdc.noaa.gov/paleo/study/23031>. The BARCAST code is ©Werner and Tingley (2015).

References

- Altekar, G., Dwarkadas, S., Huelsenbeck, J. P., and Ronquist, F.: Parallel Metropolis coupled Markov chain Monte Carlo for Bayesian phylogenetic inference, *Bioinformatics*, 20, 407–415, doi:10.1093/bioinformatics/btg427, <http://bioinformatics.oxfordjournals.org/content/20/3/407.abstract>, 2004.
- 720 Anchukaitis, K. J., D'Arrigo, R. D., Andreu-Hayles, L., Frank, D., Verstege, A., Curtis, A., Buckley, B. M., Jacoby, G. C., and Cook, E. R.: Tree-Ring-Reconstructed Summer Temperatures from Northwestern North America during the Last Nine Centuries, *Journal of Climate*, 26, 3001–3012, doi:10.1175/jcli-d-11-00139.1, 2013.
- Babst, F., Poulter, B., Bodesheim, P., Mahecha, M. D., and Frank, D. C.: Improved tree-ring archives will support earth-system science, *Nature Ecology & Evolution*, 1, 1–2, 2017.
- 725 Barclay, D. J., Wiles, G. C., and Calkin, P. E.: A 1119-year tree-ring-width chronology from western Prince William Sound, southern Alaska, *The Holocene*, 9, 79–84, doi:10.1191/095968399672825976, 1999.
- Belt, S. T., Vare, L. L., Massé, G., Manners, H. R., Price, J. C., MacLachlan, S. E., Andrews, J. T., and Schmidt, S.: Striking similarities in temporal changes to spring sea ice occurrence across the central Canadian Arctic Archipelago over the last 7000 years, *Quaternary Science Reviews*, 29, 3489 – 3504, doi:10.1016/j.quascirev.2010.06.041, aPEX: Arctic Palaeoclimate and its Extremes, 2010.
- 730 Berben, S. M. P., Husum, K., Cabedo-Sanz, P., and Belt, S. T.: Holocene sub-centennial evolution of Atlantic water inflow and sea ice distribution in the western Barents Sea, *Climate of the Past*, 10, 181–198, doi:10.5194/cp-10-181-2014, <http://www.clim-past.net/10/181/2014/>, 2014.
- Björklund, J. A., Gunnarson, B. E., Seftigen, K., Esper, J., and Linderholm, H. W.: Blue intensity and density from northern Fennoscandian tree rings, exploring the potential to improve summer temperature reconstructions with earlywood information, *Climate of the Past*, 10, 877–885, doi:10.5194/cp-10-877-2014, 2014.
- 735 Briffa, K. R., Jones, P. D., and Schweingruber, F. H.: Summer temperature patterns over Europe: a reconstruction from 1750 AD based on maximum latewood density indices of conifers, *Quaternary Research*, 30, 36–52, 1988.
- Briffa, K. R., Shishov, V. V., Melvin, T. M., Vaganov, E. A., Grudd, H., Hantemirov, R. M., Eronen, M., and Naurzbaev, M. M.: Trends in recent temperature and radial tree growth spanning 2000 years across northwest Eurasia, *Phil. Trans. R. Soc. B*, 363, 2271–2284, 2008.
- 740 Briffa, K. R., Melvin, T. M., Osborn, T. J., Hantemirov, R. M., Kirilyanov, A. V., Mazepa, V. S., Shiyatov, S. G., and Esper, J.: Reassessing the evidence for tree-growth and inferred temperature change during the Common Era in Yamalia, northwest Siberia, *Quaternary Science Reviews*, 72, 83–107, doi:10.1016/j.quascirev.2013.04.008, 2013.
- Büntgen, U., Trnka, M., Krusic, P. J., Kyncl, T., Kyncl, J., Luterbacher, J., Zorita, E., Ljungqvist, F. C., Auer, I., Konter, O., Schneider, L., Tegel, W., Stepanek, P., Brönniman, S., Hellmann, L., Nievergelt, D., and Esper, J.: Tree-Ring Amplification of the Early Nineteenth-Century Summer Cooling in Central Europe, *Journal of Climate*, 28, 5272–5288, 2015.
- 745 Chaudhuri, P. and Marron, J. S.: SiZer for exploration of structures in curves, *Journal of the American Statistical Association*, 94, 807–823, 1997.
- Christiansen, B.: Reconstructing the NH mean temperature: Can underestimation of trends and variability be avoided?, *Journal of Climate*, 24, 674–692, 2011.
- 750 Christiansen, B. and Ljungqvist, F. C.: Challenges and perspectives for large-scale temperature reconstructions of the past two millennia, *Reviews of Geophysics*, 55, 2017.

- Clague, J. J., Luckman, B. H., Van Dorp, R. D., Gilbert, R., Froese, D., Jensen, B. J., and Reyes, A. V.: Rapid changes in the level of Kluane Lake in Yukon Territory over the last millennium, *Quaternary Research*, 66, 342–355, doi:10.1016/j.yqres.2006.06.005, 2006.
- 755 Comboul, M., Emile-Geay, J., Evans, M. N., Mirnateghi, N., Cobb, K. M., and Thompson, D. M.: A probabilistic model of chronological errors in layer-counted climate proxies: applications to annually banded coral archives, *Climate of the Past*, 10, 825–841, doi:10.5194/cp-10-825-2014, <http://www.clim-past.net/10/825/2014/>, 2014.
- Comiso, J. C., Parkinson, C. L., Gersten, R., and Stock, L.: Accelerated decline in the Arctic sea ice cover, *Geophysical Research Letters*, 35, 2008.
- 760 Cook, E. R., Briffa, K. R., and Jones, P. D.: Spatial regression methods in dendroclimatology – A review and comparison of 2 techniques, *International Journal of Climatology*, 14, 379–402, 1994.
- Cook, T. L., Bradley, R. S., Stoner, J. S., and Francus, P.: Five thousand years of sediment transfer in a high arctic watershed recorded in annually laminated sediments from Lower Murray Lake, Ellesmere Island, Nunavut, Canada, *Journal of Paleolimnology*, 41, 77–94, doi:10.1007/s10933-008-9252-0, 2009.
- Curry, J. A., Schramm, J. L., and Ebert, E. E.: Sea ice-albedo climate feedback mechanism, *Journal of Climate*, 8, 240–247, 1995.
- 765 D’Arrigo, R. D., Cook, E. R., Wilson, R. J., Allan, R., and Mann, M. E.: On the variability of ENSO over the past six centuries, *Geophys. Res. Lett.*, 32, doi:10.1029/2004GL022055, 2005.
- Davi, N.: Boreal temperature variability inferred from maximum latewood density and tree-ring width data, Wrangell Mountain region, Alaska, *Quaternary Research*, doi:10.1016/s0033-5894(03)00115-7, 2003.
- 770 Divine, D. and Dick, C.: Historical variability of sea ice edge position in the Nordic Seas, *Journal of Geophysical Research*, 111, C01 001, doi 10.1029/2004JC002851, 2006.
- Divine, D. V., Isaksson, E., Godtlielsen, F., Martma, T., Meijer, H., Moore, J., Pohjola, V., and van de Wal, R. S. W.: Thousand years of winter surface air temperature variations in Svalbard and northern Norway reconstructed from ice core data, *Polar Research*, 30, doi:10.3402/polar.v30i0.7379, 2011.
- Divine, D. V., Godtlielsen, F., and Rue, H.: A modelling approach to assessing the timescale uncertainties in proxy series with chronological errors, *Climate of the Past Discussions*, 8, 31–61, doi:10.5194/cpd-8-31-2012, <http://www.clim-past-discuss.net/8/31/2012/>, 2012.
- 775 Dobrovolný, P., Moberg, A., Wilson, R., Brázdil, R., Pfister, C., Glaser, R., van Engelen, A., Limanówka, D., Kiss, A., Riemann, D., Halíčková, M., Macková, J., Luterbacher, J., and Böhm, R.: Temperature reconstruction of Central Europe derived from documentary evidence since AD 1500, *Climatic Change*, 101, 69–107, 2010.
- D’Arrigo, R., Wilson, R., and Jacoby, G.: On the long-term context for late twentieth century warming, *Journal of Geophysical Research*, 780 111, doi:10.1029/2005jd006352, 2006.
- Earl, D. J. and Deem, M. W.: Parallel tempering: Theory, applications, and new perspectives, *Physical Chemistry Chemical Physics*, 7, 3910–3916, doi:10.1039/B509983H, <http://dx.doi.org/10.1039/B509983H>, 2005.
- Emile-Geay, J. and Tingley, M.: Inferring climate variability from nonlinear proxies: application to palaeo-ENSO studies, *Climate of the Past*, 12, 31–50, 2016.
- 785 Esper, J., Frank, D., Timonen, M., Zorita, E., Wilson, R., Luterbacher, J., Holzkämper, S., Fischer, N., Wagner, S., Nievergelt, D., Verstege, A., , and Büntgen, U.: Orbital forcing of tree-ring data, *Nature Climate Change*, doi:10.1038/NCLIMATE1589, 2012.
- Esper, J., Schneider, L., Smerdon, J. E., Schöne, B. R., and Büntgen, U.: Signals and memory in tree-ring width and density data, *Dendrochronologia*, 35, 62–70, 2015.

- Fischer, H., Werner, M., Wagenbach, D., Schwager, M., Thorsteinsson, T., Wilhelms, F., Kipfstuhl, J., and Sommer, S.: Little ice age clearly recorded in northern Greenland ice cores, *Geophysical Research Letters*, 25, 1749–1752, doi:10.1029/98GL01177, 1998.
- 790 Frank, D., Esper, J., and Cook, E.: On variance adjustments in tree-ring chronology development, *Tree rings in archaeology, climatology and ecology*, TRACE, 4, 56–66, 2006.
- Franke, J., Frank, D., Raible, C. C., Esper, J., and Brönnimann, S.: Spectral biases in tree-ring climate proxies, *Nature Climate Change*, 3, 360–364, doi:10.1038/NCLIMATE1816, 2013.
- 795 Gneiting, T. and Raftery, A. E.: Strictly proper scoring rules, prediction, and estimation, *Journal of the American Statistical Association*, 102, 359–378, 2007.
- Gómez-Navarro, J. J., Werner, J., Wagner, S., Luterbacher, J., and Zorita, E.: Establishing the skill of climate field reconstruction techniques for precipitation with pseudoproxy experiments, *Climate Dynamics*, 45, 1395–1413, 2015.
- Grinsted, A., Moore, J. C., Pohjola, V., Martma, T., and Isaksson, E.: Svalbard summer melting, continentality, and sea ice extent from the Lomonosovfonna ice core, *Journal of Geophysical Research*, 111(D10), D07 110, doi:10.1029/2005JD006494, 2006.
- 800 Grinsted, A., Moore, J. C., and Jevrejeva, S.: Reconstructing sea level from paleo and projected temperatures 200 to 2100 AD, *Climate Dynamics*, 34, 461–472, 2010.
- Grootes, P. and Stuiver, M.: Oxygen 18/16 variability in Greenland snow and ice with 10^{-3} – 10^{-5} -year time resolution, *Journal of Geophysical Research*, 102(C12), 26 455–26 470, doi:10.1029/97JC00880, 1997.
- 805 Hanhijärvi, S., Tingley, M. P., and Korhola, A.: Pairwise comparisons to reconstruct mean temperature in the Arctic Atlantic Region over the last 2,000 years, *Climate Dynamics*, 41, 2039–2060, 2013.
- Harris, I., Jones, P., Osborn, T., and Lister, D.: Updated high-resolution grids of monthly climatic observations – the CRU TS3.10 Dataset, *International Journal of Climatology*, 34, 623–642, doi:10.1002/joc.3711, 2014.
- Helama, S., Vartiainen, M., Holopainen, J., Mäkelä, H., Kolström, T., and Meriläinen, J.: A palaeotemperature record for the Finnish Lakeland based on microdensitometric variations in tree rings, *Geochronometria*, 41, doi:10.2478/s13386-013-0163-0, 2014.
- 810 Hersbach, H.: Decomposition of the Continuous Ranked Probability Score for Ensemble Prediction Systems, *Weather and Forecasting*, 15, 559–570, 2000.
- Hoffmann, G., Jouzel, J., and Johnsen, S.: Deuterium excess record from central Greenland over the last millennium: Hints of a North Atlantic signal during the Little Ice Age, *Journal of Geophysical Research*, 106, 14 265–14 274, doi:10.1029/2000JD900585, 2001.
- 815 Huguen, K. A., Overpeck, J. T., and Anderson, R. F.: Recent warming in a 500-year palaeotemperature record from varved sediments, Upper Soper Lake, Baffin Island, Canada, *The Holocene*, 10, 9–19, doi:10.1191/095968300676746202, <http://hol.sagepub.com/content/10/1/9.abstract>, 2000.
- Hughes, M. K., Vaganov, E. A., Shiyatov, S., Touchan, R., and Funkhouser, G.: Twentieth-century summer warmth in northern Yakutia in a 600-year context, *Holocene*, 9, 629–634, 1999.
- 820 Hunke, E. C., Lipscomb, W. H., and Turner, A. K.: Sea-ice models for climate study: retrospective and new directions, *Journal of Glaciology*, 56, 1162–1172, doi:10.3189/002214311796406095, 2010.
- IPCC: *Climate Change 2013: The Physical Science Basis*. Contribution of Working Group I to the Fifth Assessment Report of the Intergovernmental Panel on Climate Change, Cambridge University Press, Cambridge, United Kingdom and New York, NY, USA, doi:10.1017/CBO9781107415324, www.climatechange2013.org, 2013.
- 825 Jacoby, G. C. and D’Arrigo, R.: Reconstructed Northern Hemisphere annual temperature since 1671 based on high-latitude tree-ring data from North America, *Climatic Change*, 14, 39–59, doi:10.1007/bf00140174, 1989.

- Jones, P. D., Lister, D. H., Osborn, T. J., Harpham, C., Salmon, M., and Morice, C. P.: Hemispheric and large-scale land surface air temperature variations: An extensive revision and an update to 2010, *Journal of Geophysical Research*, 117, D05 127, doi:10.1029/2011JD017139, 2012.
- 830 Kaufman, D. S., Schneider, D. P., McKay, N. P., Ammann, C. M., Bradley, R. S., Briffa, K. R., Miller, G. H., Otto-Bliesner, B. L., Overpeck, J. T., Vinther, B. M., and 2k Project Members, A. L.: Recent Warming Reverses Long-Term Arctic Cooling, *Science*, 325, 1236–1239, 2009.
- Kinnard, C., Zdanowicz, C. M., Fisher, D. A., Isaksson, E., de Vernal, A., and Thompson, L. G.: Reconstructed changes in Arctic sea ice over the past 1,450 years, *Nature*, 479, 509–512, doi:10.1038/nature10581, 2011.
- 835 Lamoureux, S. F. and Bradley, R. S.: A late Holocene varved sediment record of environmental change from northern Ellesmere Island, Canada, *Journal of Paleolimnology*, 16, 239–255, doi:10.1007/BF00176939, 1996.
- Leopardi, P.: A partition of the unit sphere into regions of equal area and small diameter, *Electronic Transactions on Numerical Analysis*, 25, 309–327, 2006.
- Li, Z., Protopopescu, V. A., Arnold, N., Zhang, X., and Gorin, A.: Hybrid parallel tempering and simulated annealing method, *Applied Mathematics and Computation*, 212, 216–228, doi:10.1016/j.amc.2009.02.023, 2009.
- 840 Ljungqvist, F., Krusic, P. J., Brattström, G., and Sundqvist, H. S.: Northern Hemisphere temperature patterns in the last 12 centuries, *Climate of the Past*, 8, 227–249, 2012.
- Ljungqvist, F. C., Krusic, P. J., Sundqvist, H. S., Zorita, E., Brattström, G., and Frank, D.: Northern Hemisphere hydroclimate variability over the past twelve centuries, *Nature*, 532, 94–98, 2016.
- 845 Lorenz, E. N.: Empirical orthogonal functions and statistical weather prediction, Tech. Rep. 1, Massachusetts Institute of Technology, 1956.
- Luterbacher, J., Werner, J. P., Smerdon, J. E., Fernández-Donado, L., González-Rouco, F. J., Barriopedro, D., Ljungqvist, F. C., Büntgen, U., Zorita, E., Wagner, S., Esper, J., McCarroll, D., Toreti, A., Frank, D., Jungclauss, J. H., Barriendos, M., Bertolin, C., Bothe, O., Brázdil, R., Camuffo, D., Dobrovolný, P., Gagen, M., García-Bustamante, E., Ge, Q., Gómez-Navarro, J. J., Guiot, J., Hao, Z., Hegerl, G. C., Holmgren, K., Klimenko, V. V., Martín-Chivelet, J., Pfister, C., Roberts, N., Schindler, A., Schurer, A., Solomina, O., von Gunten, L., Wahl, E., Wanner, H., Wetter, O., Xoplaki, E., Yuan, N., Zanchettin, D., Zhang, H., and Zerefos, C.: European summer temperatures since Roman times, *Environmental Research Letters*, 11, 024 001, <http://stacks.iop.org/1748-9326/11/i=2/a=024001>, 2016.
- 850 MacDonald, G. M., Case, R. A., and Szeicz, J. M.: A 538-Year Record of Climate and Treeline Dynamics from the Lower Lena River Region of Northern Siberia, Russia, *Arctic and Alpine Research*, 30, 334, doi:10.2307/1552005, 1998.
- Maslanik, J., Stroeve, J., Fowler, C., and Emery, W.: Distribution and trends in Arctic sea ice age through spring 2011, *Geophysical Research Letters*, 38, doi:10.1029/2011GL047735, L13502, 2011.
- 855 Masson-Delmotte, V., Landais, A., Stievenard, M., Cattani, O., Falourd, S., Jouzel, J., Johnsen, S. J., Dahl-Jensen, D., Sveinbjornsdottir, A., White, J. W. C., Popp, T., and Fischer, H.: Holocene climatic changes in Greenland: Different deuterium excess signals at Greenland Ice Core Project (GRIP) and NorthGRIP, *Journal of Geophysical Research*, 110(D9), 14 102, doi:10.1029/2004JD005575, 2005.
- McCarroll, D., Loader, N. J., Jalkanen, R., Gagen, M. H., Grudd, H., Gunnarson, B. E., Kirchhefer, A. J., Friedrich, M., Linderholm, H. W., Lindholm, M., Boettger, T., Los, S. O., Remmele, S., Kononov, Y. M., Yamazaki, Y. H., Young, G. H., and Zorita, E.: A 1200-year multiproxy record of tree growth and summer temperature at the northern pine forest limit of Europe, *The Holocene*, 23, 471–484, doi:10.1177/0959683612467483, 2013.
- 860 McKay, N. P. and Kaufman, D. S.: An extended Arctic proxy temperature database for the past 2,000 years, *Scientific Data*, 1, 140 026, doi:10.1038/sdata.2014.26, 2014.

- 865 Meier, W. N., Hovelsrud, G. K., van Oort, B. E., Key, J. R., Kovacs, K. M., Michel, C., Haas, C., Granskog, M. A., Gerland, S., Perovich, D. K., Makshtas, A., and Reist, J. D.: Arctic sea ice in transformation: A review of recent observed changes and impacts on biology and human activity, *Reviews of Geophysics*, 52, 185–217, doi:10.1002/2013RG000431, 2013RG000431, 2014.
- Melvin, T. M., Grudd, H., and Briffa, K. R.: Potential bias in “updating” tree-ring chronologies using regional curve standardisation: Re-processing 1500 years of Torneträsk density and ring-width data, *The Holocene*, 23, 364–373, doi:10.1177/0959683612460791, 2013.
- 870 Miettinen, A., Divine, D. V., Husum, K., Koç, N., and Jennings, A.: Exceptional ocean surface conditions on the SE Greenland shelf during the Medieval Climate Anomaly, *Paleoceanography*, 30, 1657–1674, doi:10.1002/2015PA002849, 2015PA002849, 2015.
- Miller, G. H., Alley, R. B., Brigham-Grette, J., Fitzpatrick, J. J., Polyak, L., Serreze, M. C., and White, J. W.: Arctic amplification: can the past constrain the future?, *Quaternary Science Reviews*, 29, 1779–1790, 2010.
- Mitchell, J., Dzerdzeevskii, B., and Flohn, H.: Climatic change: report of a working group of the Commission for Climatology, Technical
875 Note 79, World Meteorological Organisation, 1966.
- Moore, J., Hughen, K., Miller, G., and Overpeck, J.: Little Ice Age recorded in summer temperature reconstruction from varved sediments of Donard Lake, Baffin Island, Canada, *Journal of Paleolimnology*, 25, 503–517, doi:10.1023/A:1011181301514, 2001.
- Müller, J., Werner, K., Stein, R., Fahl, K., Moros, M., and Jansen, E.: Holocene cooling culminates in sea ice oscillations in Fram Strait, *Quaternary Science Reviews*, 47, 1–14, 2012.
- 880 Nilsen, T., Werner, J. P., and Divine, D. V.: How wrong are climate field reconstruction techniques in reconstructing a climate with long range memory?, in prep.
- Nilsen, T., Rypdal, K., and Fredriksen, H.-B.: Are there multiple scaling regimes in Holocene temperature records?, *Earth System Dynamics*, 7, 419–439, doi:10.5194/esd-7-419-2016, <http://www.earth-syst-dynam.net/7/419/2016/>, 2016.
- Nychka, D., Buchberger, R., Wigley, T., Santer, B. D., Taylor, K. E., and Jones, R. H.: Confidence Intervals for Trend Estimates With Autocorrelated Observations, <http://citeseerx.ist.psu.edu/viewdoc/download?doi=10.1.1.33.6828&rep=rep1&type=pdf>, (un-
885 published manuscript), 2000.
- O’Connor, F. M., Boucher, O., Gedney, N., Jones, C., Folberth, G., Coppel, R., Friedlingstein, P., Collins, W., Chappellaz, J., Ridley, J., et al.: Possible role of wetlands, permafrost, and methane hydrates in the methane cycle under future climate change: a review, *Reviews of Geophysics*, 48, 2010.
- 890 Ojala, A. E. and Alenius, T.: 10 000 years of interannual sedimentation recorded in the Lake Nautajärvi (Finland) clastic–organic varves, *Palaeogeography, Palaeoclimatology, Palaeoecology*, 219, 285 – 302, doi:<http://dx.doi.org/10.1016/j.palaeo.2005.01.002>, <http://www.sciencedirect.com/science/article/pii/S0031018205000180>, 2005.
- Opel, T., Fritzsche, D., and Meyer, H.: Eurasian Arctic climate over the past millennium as recorded in the Akademii Nauk ice core (Severnaya Zemlya), *Climate of the Past*, 9, 2379–2389, doi:10.5194/cp-9-2379-2013, <http://www.clim-past.net/9/2379/2013/>, 2013.
- 895 Østvand, L., Nilsen, T., Rypdal, K., Divine, D., and Rypdal, M.: Long-range memory in internal and forced dynamics of millenium-long climate model simulations, *Earth System Dynamics*, 5, 295–308, doi:10.5194/esd-5-295-2014, 2014.
- Overpeck, J., Hughen, K., Hardy, D., Bradley, R., Case, R., Douglas, M., Finney, B., Gajewski, K., Jacoby, G., Jennings, A., et al.: Arctic environmental change of the last four centuries, *Science*, 278, 1251–1256, 1997.
- PAGES 2k Consortium: Continental-scale temperature variability during the past two millennia, *Nature Geoscience*, 6, 339–346, 2013.
- 900 PAGES 2k Consortium: A global multiproxy database for temperature reconstructions of the Common Era, *Scientific Data*, 4, 170 088, doi:10.1038/sdata.2017.88, 2017.

- Perovich, D., Grenfell, T., Light, B., and Hobbs, P.: Seasonal evolution of the albedo of multiyear Arctic sea ice, *Journal of Geophysical Research: Oceans*, 107, 2002.
- Perovich, D., Jones, K., Light, B., Eicken, H., Markus, T., Stroeve, J., and Lindsay, R.: Solar partitioning in a changing Arctic sea-ice cover, *Annals of Glaciology*, 52, 192–196, 2011.
- Perovich, D. K., Richter-Menge, J. A., Jones, K. F., and Light, B.: Sunlight, water, and ice: Extreme Arctic sea ice melt during the summer of 2007, *Geophysical Research Letters*, 35, 2008.
- Rohde, R., Muller, R., Jacobsen, R., Muller, E., Perlmutter, S., Rosenfeld, A., Wurtele, J., Groom, D., and Wickham, C.: A new estimate of the average Earth surface land temperature spanning 1753 to 2011, *Geoinfor Geostat Overview*, 1, 1–7, 2013.
- Schneider, L., Smerdon, J. E., Büntgen, U., Wilson, R. J. S., Myglan, V. S., Kirilyanov, A. V., and Esper, J.: Revising midlatitude summer temperatures back to A.D. 600 based on a wood density network, *Geophysical Research Letters*, 42, 4556–4562, doi:10.1002/2015gl063956, 2015.
- Serreze, M. C., Holland, M. M., and Stroeve, J.: Perspectives on the Arctic’s shrinking sea-ice cover, *Science*, 315, 1533–1536, 2007.
- Shakhova, N., Semiletov, I., Salyuk, A., Yusupov, V., Kosmach, D., and Gustafsson, Ö.: Extensive methane venting to the atmosphere from sediments of the East Siberian Arctic Shelf, *Science*, 327, 1246–1250, 2010.
- Shi, F., Yang, B., Ljungqvist, F. C., and Yang, F.: Multi-proxy reconstruction of Arctic summer temperatures over the past 1400 years, *Climate Research*, 54, 113–128, 2012.
- Sigl, M., Winstrup, M., McConnell, J., Welten, K., Plunkett, G., Ludlow, F., Büntgen, U., Caffee, M., Chellman, N., Dahl-Jensen, D., et al.: Timing and climate forcing of volcanic eruptions for the past 2,500 years, *Nature*, 523, 543–549, 2015.
- Smedsrud, L. H., Sorteberg, A., and Kloster, K.: Recent and future changes of the Arctic sea-ice cover, *Geophysical Research Letters*, 35, 2008.
- Thomas, E. K. and Briner, J. P.: Climate of the past millennium inferred from varved proglacial lake sediments on northeast Baffin Island, Arctic Canada, *Journal of Paleolimnology*, 41, 209–224, doi:10.1007/s10933-008-9258-7, 2009.
- Tingley, M. P.: A Bayesian ANOVA scheme for calculating climate anomalies, with applications to the instrumental temperature record, *Journal of Climate*, 25, 777–791, doi:10.1175/JCLI-D-11-00008.1, 2012.
- Tingley, M. P. and Huybers, P.: A Bayesian Algorithm for Reconstructing Climate Anomalies in Space and Time. Part I: Development and Applications to Paleoclimate Reconstruction Problems, *Journal of Climate*, 23, 2759–2781, doi:10.1175/2009JCLI3015.1, 2010a.
- Tingley, M. P. and Huybers, P.: A Bayesian Algorithm for Reconstructing Climate Anomalies in Space and Time. Part II: Comparison with the Regularized Expectation-Maximization Algorithm, *Journal of Climate*, 23, 2782–2800, doi:10.1175/2009JCLI3016.1, 2010b.
- Tingley, M. P. and Huybers, P.: Recent temperature extremes at high northern latitudes unprecedented in the past 600 years, *Nature*, 496, 201–205, doi:10.1038/nature11969, 2013.
- Tipton, J., Hooten, M., Pederson, N., Tingley, M., and Bishop, D.: Reconstruction of late Holocene climate based on tree growth and mechanistic hierarchical models, *Environmetrics*, 27, 42–54, doi:10.1002/env.2368, <http://dx.doi.org/10.1002/env.2368>, env.2368, 2016.
- Vermeer, M. and Rahmstorf, S.: Global sea level linked to global temperature, *Proceedings of the National Academy of Sciences*, 106, 21 527–21 532, 2009.
- Vinther, B., Jones, P., Briffa, K., Clausen, H., Andersen, K., Dahl-Jensen, D., and Johnsen, S.: Climatic signals in multiple highly resolved stable isotope records from Greenland, *Quaternary Science Reviews*, 29, 522 – 538, doi:<http://dx.doi.org/10.1016/j.quascirev.2009.11.002>, <http://www.sciencedirect.com/science/article/pii/S0277379109003655>, 2010.

- von Storch, H., Zorita, E., Jones, J. M., Dimitriev, Y., González-Rouco, F., and Tett, S. F. B.: Reconstructing past climate from noisy data, 940 *Science*, 306, 679–682, 2004.
- Walsh, J. E., Fetterer, F., Scott Stewart, J., and Chapman, W. L.: A database for depicting Arctic sea ice variations back to 1850, *Geographical Review*, 107, 89–107, 2017.
- Wang, J., Emile-Geay, J., Guillot, D., McKay, N. P., and Rajaratnam, B.: Fragility of reconstructed temperature patterns over the Common Era: Implications for model evaluation, *Geophysical Research Letters*, 42, 7162–7170, doi:10.1002/2015GL065265, 2015.
- 945 Weißbach, S., Wegner, A., Opel, T., Oerter, H., Vinther, B. M., and Kipfstuhl, S.: Spatial and temporal oxygen isotope variability in northern Greenland – implications for a new climate record over the past millennium, *Climate of the Past*, 12, 171–188, doi:10.5194/cp-12-171-2016, <http://www.clim-past.net/12/171/2016/>, 2016.
- Werner, J. and Tingley, M.: Technical Note: Probabilistically constraining proxy age–depth models within a Bayesian hierarchical reconstruction model, *Climate of the Past*, 11, 533–545, doi:10.5194/cpd-10-4499-2014, 2015.
- 950 Werner, J., Smerdon, J., and Luterbacher, J.: A Pseudoproxy Evaluation of Bayesian Hierarchical Modelling and Canonical Correlation Analysis for Climate Field Reconstructions over Europe, *Journal of Climate*, doi:10.1175/JCLI-D-12-00016.1, 2013.
- Wiles, G. C., D’Arrigo, R. D., Barclay, D., Wilson, R. S., Jarvis, S. K., Vargo, L., and Frank, D.: Surface air temperature variability reconstructed with tree rings for the Gulf of Alaska over the past 1200 years, *The Holocene*, 24, 198–208, doi:10.1177/0959683613516815, 2014.
- 955 Zhang, H., Werner, J., Luterbacher, J., Garcia-Bustamante, E., González-Rouco, F., Wagner, S., Zorita, E., Fraedrich, K., Jungclaus, J., and Zhu, X.: Gridded decadal warm season temperature over East Asia in the past 1200 years, in review.
- Zhang, H., Yuan, N., Esper, J., Werner, J. P., Xoplaki, E., Büntgen, U., Treydte, K., and Luterbacher, J.: Modified climate with long term memory in tree ring proxies, *Environmental Research Letters*, 10, 084 020, <http://stacks.iop.org/1748-9326/10/i=8/a=084020>, 2015.
- Zhang, P., Linderholm, H. W., Gunnarson, B. E., Björklund, J., and Chen, D.: 1200 years of warm-season temperature variability in central 960 Scandinavia inferred from tree-ring density, *Climate of the Past*, 12, 1297–1312, doi:10.5194/cp-12-1297-2016, 2016.